

THE BROAD-BAND NOISE CHARACTERISTICS OF SELECTED
CATAclySMIC VARIABLES (CVS), ANOMALOUS X-RAY PULSARS (AXPS)
AND SOFT GAMMA REPEATERS (SGRS)

A THESIS SUBMITTED TO
THE GRADUATE SCHOOL OF NATURAL AND APPLIED SCIENCES
OF
MIDDLE EAST TECHNICAL UNIVERSITY

BY

BAYBARS KÜLEBİ

IN PARTIAL FULFILLMENT OF THE REQUIREMENTS
FOR
THE DEGREE OF MASTER OF SCIENCE
IN
PHYSICS

DECEMBER 2006

Approval of the Graduate School of Natural and Applied Sciences.

Prof. Dr. Canan Özgen
Director

I certify that this thesis satisfies all the requirements as a thesis for the degree of Master of Science.

Prof. Dr. Sinan Bilikmen
Head of Department

This is to certify that we have read this thesis and that in our opinion it is fully adequate, in scope and quality, as a thesis for the degree of Master of Science.

Assoc. Prof. Dr. Şölen
Balman
Supervisor

Examining Committee Members

Prof. Dr. Ümit Kızılođlu (METU,PHYS)_____

Assoc. Prof. Dr. Şölen Balman (METU,PHYS)_____

Prof. Dr. Altan Baykal (METU,PHYS)_____

Prof. Dr. Nilgün Kızılođlu (METU,PHYS)_____

Assist. Prof. Dr. S. Çađdaş İnam (BAŞKENT,EEE)_____

“I hereby declare that all information in this document has been obtained and presented in accordance with academic rules and ethical conduct. I also declare that, as required by these rules and conduct, I have fully cited and referenced all material and results that are not original to this work.”

Name Surname : BAYBARS KÜLEBİ

Signature :

ABSTRACT

THE BROAD-BAND NOISE CHARACTERISTICS OF SELECTED CATAclySMIC VARIABLES (CVS), ANOMALOUS X-RAY PULSARS (AXPS) AND SOFT GAMMA REPEATERS (SGRS)

KÜLEBİ, Baybars

M.S., Department of Physics

Supervisor: Assoc. Prof. Dr. Şölen Balman

December 2006, 62 pages.

In this work present the broad-band noise structure in the 2-60 keV data of Cataclysmic Variables (CVs) with Anomalous X-Ray Pulsars (AXPs) and Soft Gamma Repeaters (SGRs). We analyzed Rossi X-ray Timing Explorer (RXTE) PCA data and derived time series from 27 CVs, 4 AXPs and 1 SGR using the RXTE archive. In general, CVs of different types all show broad band noise which can be fitted with power laws, using exponential cut-offs, and Lorentzians in a similar way to power spectral (noise) characteristics of X-ray Binaries (XRBs). In general terms the power spectra show a power law index of $(-1.2-2)$. A rather large scale flattening of the power spectra exists in nonmagnetic systems in the low to very low frequency range. We observe that in low and high states/outbursts the noise in the high frequency range and low frequency range is changed. CVs show considerably low frequency noise. In addition, we recovered several possible QPOs in the X-ray wavelengths from CVs mainly from Intermediate Polar systems. AXP and SGR sources which are thought to be powered

by either magnetic decay or accretion show band limited noise in their low frequencies. We also correlated their equal time interval noise characteristic with their burst states and discovered that in the two AXPs (1E 2259+586, 1E 1048.1-5937) noise correlates with their bursts.

Keywords: Cataclysmic variables, neutron stars, broad-band noise, quasi periodic oscillation

ÖZ

GENİŞ FREKANS BANDINDA SEÇİLMİŞ KATAKLİSMİK DEĞİŞKEN, ANORMAL X-IŞINI ATARICALARI VE YUMUŞAK GAMA IŞINI OBJELERİNİN GÜRÜLTÜ ANALİZİ

KÜLEBİ, Baybars

Yüksek Lisans , Fizik Bölümü

Tez Yöneticisi: Assoc. Prof. Dr. Şölen Balman

Aralık 2006, 62 sayfa.

Bu çalışmada KatakliSMik Değişkenler'in (CVler) Sıradışı X-ışını Pulsar'ı (AXP) ve bir Yumuşak Gama Yineleyici'nin (SGR) 2-60 keV aralığındaki güç tayfı geniş bant gürültü karakteristikleri incelenmektedir. Rossi X-ray Timing Explorer (RXTE) uydusunun arşivinden alınmış 27 CV'nin, 4 AXP'nin ve 1 SGR'in Proportional Counter Array (PCA) verisi analiz edilmiştir. Genel olarak değişik türlerden CVlerde geniş bantta güç kanunu, eksponansiyel kesilme ve Lorentzian modelleri ile açıklanabilen gürültü gözlenmektedir. Aynı özellikteki gürültüler X-ışını çift yıldız sistemlerinde de görülmektedir. Sonuçta güç tayfları(-) 1.2-2 eğime sahip olmakla beraber, manyetik olmayan sistemlerde çok düşük frekanslarda eğimlerinde düzleşme gözlenmektedir. Ayrıca bu kaynakların yüksek/patlama ve düşük parlaklık evrelerinde gürültü, yüksek frekanslar ve düşük frekanslar arasında yer değiştirmektedir ve düşük frekanslarda gürültüye sahip olan bu CVler, tayflarında kuasi-periyodik salınımlar da göstermektedirler. Salınım mekanizmaları manyetik bozunma ya da madde aktarımı olduğu düşünülen AXP ve

SGRların ise geniş bant aralığında gürültüye sahip oldukları ortaya çıkmıştır. 1E 2259+586, 1E 1048.1-5937 AXPleri için eşit dönemlerde incelenen bu gürültülerin patlama zamanlarına bağlı olarak değiştikleri de gözlemlenmiştir.

Anahtar Kelimeler: Katakлизмik Değişkenler, nötron yıldızları, geniş bant gürültü, kuasi periyodik salınım

ACKNOWLEDGMENTS

I would like to express my deepest gratitude to Assoc. Prof. Dr. Şölen Balman for her guidance and insight throughout the research.

I would like to thank Prof. Dr. Altan Baykal for his fruitful discussions and helpful suggestions. I also thank Elif Beklen for her collaboration during the CV analyses.

I express my gratitude to Oya Külebi for raising me with the incentive to pursue knowledge and Ekin Özenci for her tireless encouragement.

I thank my friends and colleagues in METU Astrophysics Group and TÜBİTAK High Energy Astrophysics Unit for their support. I acknowledge a scholarship provided by Turkish Scientific Research Council (TÜBİTAK).

TABLE OF CONTENTS

ABSTRACT	v
ÖZ	vii
ACKNOWLEDGMENTS	ix
TABLE OF CONTENTS	x
LIST OF TABLES	xii
LIST OF FIGURES	xiii
1 INTRODUCTION	1
1.1 Cataclysmic Variables	1
1.1.1 Classes of Cataclysmic Variables	1
1.1.2 Theoretical overview	3
1.1.3 Accretion in the absence of a magnetic field	6
1.1.4 Accretion in the vicinity of a magnetic field	7
1.2 AXPs & SGRs	8
1.2.1 Breaking index, spin down age and $P - \dot{P}$ diagram	8
1.2.2 AXP SGR properties	12
1.2.3 Magnetar model	13
1.2.4 Fallback disk model and beyond	15
2 RXTE OBSERVATIONS AND DATA ANALYSIS	24
2.1 RXTE Observations	24
2.2 Fourier Techniques in X-ray Timing	26

3	RESULTS	40
3.1	Results for CVs	40
3.1.1	Polars	40
3.1.2	Intermediate Polars	41
3.1.3	Non-magnetic CVs	41
3.2	Results for AXPs and SGRs	41
4	CONCLUSION	58
4.1	CVs	58
4.2	AXPs and SGRs	60
	REFERENCES	63

LIST OF TABLES

1.1	Physical properties of CVs that are discussed in this work from Downes et. al. (2001)	20
1.2	Physical properties of CVs cont'd from Table 1.1	21
1.3	Timing properties of AXPs and SGRs.	22
1.4	Spectral properties of AXPs and SGRs. Luminosities are 2-10 keV integrated.	23
2.1	Log of CV observations in this paper.	34
2.2	AXPs and SGRs analyzed in this work.	35
3.1	Parameters and QPOs derived from the fits applied on the power spectra using Lorentzian and Power Law models	44
3.2	Parameters and QPOs cont'd from Table 3.1	45

LIST OF FIGURES

1.1	Roche lobe diagram	19
2.1	High versus low state lightcurve of SS Cyg	36
2.2	High versus low state lightcurve of AM Her	37
2.3	Burst epoch lightcurve of 1E 2259+586.	38
2.4	Burst epoch lightcurve of 1E 1048-5937	39
3.1	Broad-band noise of polars.	46
3.2	Broad-band noise of intermediate polars.	47
3.3	Broad-band noise of intermediate polars(cont'd).	48
3.4	Broad-band noise of non-magnetic CVs.	49
3.5	Broad-band noise of AXP 1E 1048-5937	50
3.6	Broad-band noise of AXP 1E 1048-5937 (cont'd)	51
3.7	Broad-band noise of 1E 2259+586	52
3.8	Broad-band noise of 1E 2259+586	52
3.9	Broad-band noise of 1E 2259+586 (cont'd)	53
3.10	Broad-band noise of RXS J1708-40	54
3.11	Broad-band noise of 1E 1841-045	55
3.12	Broad-band noise of SGR 1806-20	56
3.13	Broad-band noise of SGR 1806-20(cont'd)	57

CHAPTER 1

INTRODUCTION

The different families of objects which will be discussed in this work are Cataclysmic Variables (CVs) Anomalous X-Ray Pulsars (AXPs) Soft Gamma Repeaters (SGRs). Each has their own exotic properties.

Broad-band noise can be indicate physical details of these kinds of systems. In this work we analyzed RXTE data to investigate the noise properties of CVs, AXPs and SGRs. In this chapter, emission mechanisms are discussed. Timing analysis basics and data analysis conventions in X-ray astrophysics is explained in Chapter 2. And finally in Chapters 3 and 4 results are presented.

1.1 Cataclysmic Variables

1.1.1 Classes of Cataclysmic Variables

Cataclysmic Variables (CVs) are binary systems that consist of a white dwarf (WD) and a low mass main sequence star. The former is called the primary, accretes matter from the low mass secondary, the latter component. Their periods are around 1 - 10 hours and they revolve in very small orbits, roughly the size of

Earth Moon system.

The classification of CVs is very complex because of their diverse observational properties but a more physical approach can be adopted. First of all they are divided into magnetic and non-magnetic types, and CVs are divided into four classes, namely; classical novae, recurrent novae, dwarf novae and nova-like variables.

Classical novae (CN) are the most conventional type of CV in which one luminous eruption occurs over a long period of time. These eruptions' observational properties include an increase in optical brightness (6 - 19 magnitudes) and a slow decline in the order of ten to a hundred days, and they recur over a period of 10^4 years. These bursts are assumed to be *thermonuclear runaways* from hydrogen that is accreting on the WD surface (Warner 95).

Recurrent novae (RN) are the counterparts of CN which consist of more periodic bursts. This property is assumed to be a result of high accretion rate.

Dwarf novae (DN) comprise less luminous outbursts (2 - 5 mag increase) which tend to repeat themselves on fast time scales, depending on the object typical timescale can be from ten days to an order of ten years. Burst durations tend to lie between 2 - 20 days and show a correlation with occurrence periodicities. These bursts are results of a temporary increase in accretion rate that is caused by disk instability. The DN is also divided into subclasses due to their varied morphology of their outburst light curves. In which, *SU UMa* type stars have

occasional giant outbursts that are more luminous and last longer, *Z Cam* stars acquire intermediate level luminosities with lack of bursting activity for an order of tens of days to years and finally *U Gem* type entails all the DN that are not included in the other classes.

Nova-like variables (NL) do not have outbursts which may be a result of long time scale of CN burst so this class possibly includes pre or post-novae.

Magnetic CVs are divided into polars and intermediate polars. Magnetic field around the WD disrupts the accretion disk and redirects it to its poles. *Polars* have the strongest magnetic fields and due to that the WD rotates synchronously with the binary period, whereas *intermediate polars (IPs)* tend to comprise weaker magnetic fields, and their primaries rotate asynchronously.

1.1.2 Theoretical overview

The compact properties of CVs result in exotic effects. Namely the formation of a disk around the white dwarf hence the production of high energy photons from release of gravitational energy.

We can assume that the systems motion is circular and obeys Kepler's Law,

$$P_{orb}^2 = \frac{4\pi^2 a^3}{G(M_1 + M_2)} \quad (1.1)$$

Above a is the orbital separation and the first mass is the WD mass, second mass is secondary stars mass. Hence we look at the orbital separation;

$$a = 3.53 \times 10^{10} P_{orb}^{2/3} M_1^{1/3} (1 + q)^{1/3} \text{ cm} \quad (1.2)$$

Here the $q = M_2/M_1$, and if we plug in the values for the parameters assuming periods mentioned above, say $P_{orb} = 2$ hr and approximating the masses according to the mass of the Sun, $M_1 = M_{sun}$ and $M_2 = 0.2M_{sun}$ we end up with values smaller than the radius of the Sun, $R_{sun} = 6 \times 10^8$ cm.

If the effective potential of the system in the rotating frame is written, we end up with;

$$\Phi(\vec{R}) = -\frac{GM_1}{|\vec{R} - \vec{R}_1|} - \frac{GM_2}{|\vec{R} - \vec{R}_2|} - \frac{1}{2}(\vec{\Omega} \times \vec{R})^2 \quad (1.3)$$

the last term represents the centrifugal force and the whole potential is called the Roche lobe potential (Frank et al. 1992). In this equation \vec{R}_1 and \vec{R}_2 are distances of the point masses from the center, and $\vec{\Omega}$ is the angular frequency.

When we look at the equipotential surfaces of the Roche potential (Fig. 1.1) we resolve that there are equilibrium points. L_1 , L_2 and L_3 are unstable equilibrium points that are shown in the figure, and they are called Lagrange points. The most important one, L_1 , is called the inner Lagrange point and the equipotential surface that crosses this point is called the Roche lobe. This is the largest surface that a star can extend. If the star is any larger than its Roche lobe, its excess mass is transferred to the companion star's Roche lobe. CVs are called

semi-detached binaries, since only one of the components, the WD, is smaller than its Roche lobe, moreover the secondary extends as large as its Roche lobe. This property results in transfer of the secondary star's material on to the WD, from the Lagrange point.

From the L_1 matter falls on the WD in various possibilities depending on the structure of it. But roughly the result is the transformation of gravitational energy into photons, ranging from infrared to X-Ray frequencies. From this point of view the resulting luminosity can be expressed as,

$$L = \frac{G\dot{M}M_{WD}}{R_{WD}} \approx 2.2 \frac{\dot{M}}{10^{-9}M_{\odot}\text{yr}^{-1}} \frac{M_{WD}}{M_{\odot}} \frac{10^4\text{km}}{R_{\odot}} L_{\odot} \quad (1.4)$$

In equation (1.4) the second form is present for calculation purposes and luminosity of the sun is, $L_{\odot} = 4 \times 10^{33}\text{erg s}^{-1}$. Average accretion rates for CVs are between $10^{-11} - 10^{-9} M_{\odot} \text{ yr}^{-1}$ (Howell et al. 2001). These rates would lead to $10^{31} - 10^{34} \text{ erg s}^{-1}$ of luminosities if we simply use $1 M_{\odot}$ for the primary mass and $5,400 \text{ km}$ for the primary radius. Note that 10^{34} erg is rare for quiescence, but it corresponds to high or outburst states of CVs.

In the absence of other effects accretion will result in binary separation and an increase in the size of the Roche lobe. This increase eventually causes the binary to become detached, hence it lacks any mass transfer. However this is countered by the loss of angular momentum that is caused by magnetic braking (Verbunt &

Zwaan 1981) and gravitational radiation (Faulkner 1971). The binary separation hence the Roche lobe shrinks with the loss of angular momentum, and this effect becomes a measure for the accretion rate.

1.1.3 Accretion in the absence of a magnetic field

Accretion kinematics for semi-detached binaries is similar. The matter flows through L_1 on the orbital plane and due to the binary motion and the angular momentum conservation, the matter do not fall directly on to the compact object unless binary motion is extremely slow. The stream hence misses the WD but continues to move around the primary on the orbital plane until it hits itself. This supersonic collision results in kinetic energy dissipation and heating which in turn leads to a ring formation around the primary. This mass accumulation eventually leads to a thin disk formation (Verbunt 1982).

The matter on the disk has its respective velocities at specific Kepler radii but due to viscosity, differential rings of matter transfers angular momentum to the ring above and slows down the ring below itself. This results in outward transport of angular momentum and as a consequence innermost matter spiral down to the primary surface. Even though the physical origins of the viscosity is unaccounted for, Shakura & Sunyaev (1973) developed a successful theory with the use of parameter α .

The loss of angular momentum that eventually results in surface accretion

happens in a specific area called boundary layer. This layer is between the inner disk radius and the WD's surface, and is where the matter velocity transition between Keplerian velocity of nearly 3000 km s^{-1} to WD surface velocity of nearly 300 km/s occurs. This sudden braking of accretion material leads to heating and photon emission in X-Ray, ultraviolet and optical, which comprises up to half of the total luminosity.

1.1.4 Accretion in the vicinity of a magnetic field

Significant magnetic fields disrupt the accretion disks and further complicate the above picture. For WDs this magnetic field value is 10^4 G . Disk truncation occurs around the Alfvén radius, r_A which is defined as where the magnetic energy density is comparable to the kinetic energy density. At the Alfvén radius the particles are redirected towards the magnetic poles, hence boundary layer structures are not present in these objects. In *intermediate polars* the disk radii are larger than r_A hence the disks are present, but *polars* lack disks due to the fact that their r_A extends above their L_1 point. Due to the lack of boundary layer and the transport of the matter near the magnetic poles, the accretion area is significantly decreased. In the magnetic accretion the matter is channeled on to $10^{-4} - 10^{-3}$ of the total WD surface.

The standard model of the accretion column gives a general picture of the accretion in the magnetic CV systems. As the accreting matter impacts the

surface approximately radially in supersonic speeds, it encounters a standoff shock. This heats the plasma above the WD and it starts to cool through bremsstrahlung and cyclotron emissions (Lamb & Masters 1979). This picture of accretion column is valid for specific accretion rates, i.e. $0.1 - 10 \text{ gcm}^{-2}\text{s}^{-1}$ or $10^{-27} - 10^{-25} M_{\odot}\text{cm}^{-2}\text{yr}^{-1}$.

1.2 AXPs & SGRs

1.2.1 Breaking index, spin down age and $P - \dot{P}$ diagram

Breaking is a property that is experienced by all neutron stars (NSs) regardless of their emission properties. Whenever there is some kind of matter around a magnetic neutron star, either from stellar wind and a disk or from interstellar matter, this matter will be swept away as a consequence of magnetic field lines. When the matter that is accelerated along the field lines escape from NS's field, it carries angular momentum with it as a consequence. This breaking effect gives information about NS's magnetic field, its age and the structure of its magnetic field.

Starting with *Larmor's formula* from Jackson (1998), we can express the energy loss due to a rotating dipole magnetic field.

$$-\left(\frac{dE}{dt}\right)_{rad} = \frac{q\ddot{r}^2}{6\pi\epsilon_0c^3} \quad (1.5)$$

In CGS units this transforms as,

$$\dot{E} = \frac{2}{3c^3} \Omega^2 \ddot{\mu}^2 \quad (1.6)$$

here μ is dipole magnetic moment and for a rotating NS,

$$\mu = \mu \sin(\Omega t). \quad (1.7)$$

and that means $\ddot{\mu} = -\Omega^2 \mu$. Hence the energy loss becomes,

$$\dot{E} = -\frac{2}{3c^3} \Omega^4 \mu^2. \quad (1.8)$$

The rotational properties dictate that energy depends on the moment of inertia I , from this mechanical energy loss can also be expressed as below,

$$E = \frac{1}{2} I \Omega^2 \quad (1.9)$$

$$\dot{E} = I \Omega \dot{\Omega} \quad (1.10)$$

The spin down torque due to the magnetic dipole radiation can be reached by equating these two, and plugging in moment of inertia of a sphere, $I = 2/5 MR^2$.

$$\dot{E} = I \Omega \dot{\Omega} = -\frac{2}{3c^3} \Omega^4 \mu^2 \quad (1.11)$$

$$\dot{\Omega} = -\frac{5\Omega^3 \mu}{3MR^2 c^3} \quad (1.12)$$

From (1.7) it is easy to see that $B_S \approx \mu/R^3$ (also Longair 1994) Plugging all in we end up with,

$$B_S^2 = \frac{3\mu}{5c^3 R^4} \frac{\dot{\Omega}}{\Omega^3} \quad (1.13)$$

$$B_S = 3 \times 10^{19} (P\dot{P})^{1/2} \quad (1.14)$$

Also the characteristic time or spin down age is defined from this braking. In equation (1.12) $\dot{\Omega} \propto -\Omega^3$ for a dipole field. Here we call 3 the braking index for a dipole field. In general terms,

$$\dot{\Omega} = -k\Omega^n \quad (1.15)$$

n is called the braking index and it depends on the magnetic field, namely its multipolar structure. This index can be found for each pulsar with the help of second derivative of the angular frequency,

$$\ddot{\Omega} = -kn\Omega^{n-1}\dot{\Omega} \quad (1.16)$$

When we divide (1.16) by (1.15), we get rid of k and end up with an expression for n ,

$$n = \frac{\ddot{\Omega}\Omega}{\dot{\Omega}^2} \quad (1.17)$$

An approximate age for pulsars can be derived from these arguments by assuming that the pulsar spins down constantly, namely with a constant braking

index. This is called the spin down age can be calculated by integrating the equation (1.15) with constant n .

$$\tau_c = -\frac{\Omega}{\dot{\Omega}}(n-1) \quad \tau_c = \frac{P}{(n-1)\dot{P}} \quad (1.18)$$

The spin down effect of the pulsars is very important in the NS phenomenology. First of all, the radio pulsars are thought to be rotation powered (Manchester & Taylor 1977), moreover the evolution of all NS can be probed on a diagram of period derivative versus period. This is a natural consequence of expressions (1.14) and (1.18), namely the feasibility of expressing magnetic fields and ages of pulsars merely by these two parameters.

Even though the derivations comprise numerous assumptions, the pulsars are clustered in the $P - \dot{P}$ diagram. This is a natural consequence of the dominance of the emission mechanism mentioned above. As the pulsars age, they move in this diagram since they are spinning down. We know from equation (1.14) as pulsars spin down they become faint. They finish their evolution by passing over the proverbial death line and turning off completely. In the $P - \dot{P}$ diagram AXPs and SGRs show up as highly magnetized neutron stars.

1.2.2 AXP SGR properties

AXPs and SGRs are part of a new class of neutron stars (NSs), which their emission mechanisms commute with neither accreting X-Ray Pulsars (XPs) nor radio pulsars (PSRs). They are characterized by their rapid spin down ($10^{-13} - 10^{-11} \text{ s s}^{-1}$) and high quiescent luminosities that can not be explained by spin down mechanisms ($10^{33} - 5 \times 10^{35} \text{ erg s}^{-1}$) (Woods & Thompson 2004, and references therein). Historically these physical properties were the reason for the anomalous adjective in AXPs. There are 8 AXPs presently, which are 1E 2259+586, 1E 1048.1-5937, 4U 0142+611, RXS J170849-400910, XTE J1810-197, 1E 1841-045, AX J1845-0258 and CXOU 010043.1-721134.

Since the discovery of first AXP 1E 2259+586 (Fahlman & Gregory 1981), there have been many discussions about their source of luminosity. The most important one emerged as the fall-back disk model (van Paradijs et al. 1995; Chatterjee et al. 2000; Alpar 2001). It relies on the fact that after the supernova (SN) explosion, some of the material that lacks the escape velocity in the expanding shell falls back on the compact object. As a result the increased luminosity can be explained with mass transfer rate \dot{M} . Although very successful in explaining the luminosity, the model lacked any other evidence for the fossil disk; especially the unsatisfactory infrared and optical data in these sources hindered the efforts for this model.

SGRs demonstrate gamma ray bursts in various energy ranges in addition to the above AXP properties. This effect resulted in the first detection of an SGR 0526-66 in March 5 1979 (Ramaty et. al 1980). SGR 1900+14 , SGR 1806-20 and SGR 1627-41 are the other three that belong to this type, former two are in our galaxy and SGR 0526 is in Large Magellanic Cloud (Gaensler et al. 2001).

1.2.3 Magnetar model

The magnetar model assumes AXPs and SGRs as highly magnetized neutron stars and proposes that the magnetic dissipation is the main driving force behind the SGR bursts and X-Ray emissions. Starting with Duncan & Thompson (1992), Thompson & Duncan (1993) this idea gained momentum in the last decade with increasing observational evidence.

As the young neutron star forms, its magnetic field is amplified via $\alpha - \Omega$ dynamo process but for most of the neutron stars with periods $P_i > 30\text{ms}$ dynamo effect turns off as the progenitor cools, and NS magnetic fields end up around the order 10^{12} G. But for NS progenitors spinning as fast as convective time scale $P_i < 3\text{ms}$, the $\alpha - \Omega$ dynamo process do not cease and amplify the magnetic fields as high as 10^{16} G. These are significant values considering the critical magnetic field, which is the threshold where the quantum electrodynamics dominate and the field cyclotron lines are quantized. Using the cyclotron frequency $\omega = eB/mc$, and considering the quantum energy limit where $m_e c^2$ is comparable to $\hbar\omega$,

$$B_c = \frac{mc^2\omega}{ec} = \frac{m_e c(\hbar\omega)}{\hbar e} \approx 4.4 \times 10^{13} G \quad (1.19)$$

Thompson & Duncan (1995) argue that the magnetar magnetic fields that are larger than this critical value is responsible for the large spin downs of AXPs and SGRs. Also the magnetic dissipation on the crust that is responsible for the main source of energy in magnetars can be derived from the derivative of the total magnetic energy.

If the total magnetic energy can be expressed as,

$$E_B = \frac{1}{8\pi} \int |\vec{B}|^2 d^3x \quad (1.20)$$

and the magnetic field is known, then magnetic energy dissipation becomes,

$$(\dot{E}_B) = \frac{d}{dt} \left(\frac{1}{3} B_S^2 R^3 \right) = -\frac{2}{3} B_S \dot{B}_S R^3. \quad (1.21)$$

The unknown term is the evolution of the magnetic field $\partial B_S / \partial t$. Numerous models were proposed to address this parameter (Goldreich & Reisenegger 1992).

The magnetar model about this type of objects was based mostly on March 5 event (Duncan & Thompson 1996; Thompson & Duncan 1995). It deduces SGR burst as a novel observation, moreover it predicts the AXP bursts which occurred for 1E 2259+586 (Kaspi & Gavriil 2002) and 1E 1048.1-5937 (Gavriil et al 2002) with the consideration of AXPs as magnetars.

From spin down age and supernova remnants(SNRs) associations, these objects are considered to be young pulsars. They all lie on the galactic plane save SGR 0526-66 which is in LMC. Their periods are clustered between 5-12 seconds. It also explains the large spin down values consequently. Timing properties are on Table 1.3.

Magnetar spectra demonstrate two component morphologies, namely a black body component and a power law. The black body temperature lie between 0.4 - 0.67 keV and the power law indexes are between 1 - 4 as expressed in Table 1.4 for individual magnetars.

1.2.4 Fallback disk model and beyond

This concept proposes the falling back of a material after a supernova burst. While most of the material from the shell has the escape velocity, some quantities may lack the kinetic energy to escape the gravitational pull. Even though this model has been used in many different systems, like Michel & Dessler (1981) for radio pulsars or for the SN 1987A remnant (Meyer & Meyer-Hofmeister 1989; Meyer-Hofmeister 1992), it has been one of the significant models in explaining the emission properties of AXPs and SGRs. (Chatterjee et al. 2000; Alpar, 2001)

The advantages of this model are its relative success in explanation of period clustering and theoretical framework it proposes for the AXP infrared and optical emissions. (Hulleman et al. 2001; Wang, Chakrabarty & Kaplan 2006)

First of all, unlike binary systems the accretion is time dependent since matter source is the limited fall back material. From this fact Chatterjee et al. (2000) modeled the accretion time dependence as a power law, in which the value of the power law index depends on the opacity of the disk.

According to this model there should also be evolutionary phases of NS accreting from fall back material. In which evolutionary phase would a NS be is determined by the three important radii that were discussed in Chapter 1.1.4; the Alfvén radius r_A , the corotation radius r_{co} , and the light cylinder radius r_{lc} .

In the first case, the ordinary pulsar phase, r_A is larger than the light cylinder radius, r_{lc} hence disk do not interact with the magnetosphere. This means the disk do not contribute in any way to emission and the NS is like an ordinary pulsar.

This phase ends as pulsar spins down due to braking and corotation radius, r_{co} increases. Also with the decreasing accretion rate \dot{m} , the Alfvén radius increases. Hence r_{co} and r_A starts to approach each other, but still r_A is lot larger than corotation radius which also means spin frequency is alot larger than Keplerian frequency. Because of this NS starts to transfer angular momentum to the disk and the matter on it escapes from pulsars gravitational pull. This rapid spin down supposedly continues till an equilibrium spin frequency, but the system never reaches this spin frequency. This phase is called propeller phase of the pulsar and it's physics have been explained first by Illarionov & Syunyaev (1975).

Finally, as the corotation radius becomes comparable to the Alfén radius, pulsars spin period approaches the equilibrium period. In this phase accretion becomes more efficient and it is called the tracking phase. Here pulsar is in its brightest but \dot{m} starts to decrease with the luminosity.

The natural result of this final phase is period clustering of AXP. Since this pulsars radiate strongly only in this phase, they are subjected to a selection effect where their periods are comparable to the equilibrium radius where $r_A \approx r_{co}$.

To reach the luminosities of AXPs we would assume an accretion rate of $\dot{m} \approx 10^{14} - 10^{16} \text{ g s}^{-1}$ with regular pulsar spin down characteristics. This means in the fallback model these NSs have regular pulsar dipole fields of $10^{12} - 10^{13}$.

Another indicator of accretion is the noisy timing instead of steady spin down. This torque transfer to the star is a natural result for all accreting sources (Lipunov 1992). Baykal et al. (2000) used this fact in their investigation of 1E 1048.1-5937 and concluded that its timing noise consistent with accreting sources.

Currently a new generation hybrid model has put forth for fallback disk model that can be referred to as best of the both worlds (Ekşi & Alpar 2003; Ertan & Alpar 2003; Ertan, Göğüş & Alpar, 2006). In this model the NS have a high quadrupole field ($10^{14} - 10^{15} \text{ G}$) responsible for magnetar like burst, and a regular dipole field ($10^{12} - 10^{13} \text{ G}$) that interacts with the fallback disk. This model not only entails the burst phenomenology of magnetars with the spin period selection effect and optical/IR radiation arises from the fallback disk, but also explains the

post-burst enhanced X-Ray luminosity with the relaxation of the pushed back disk.

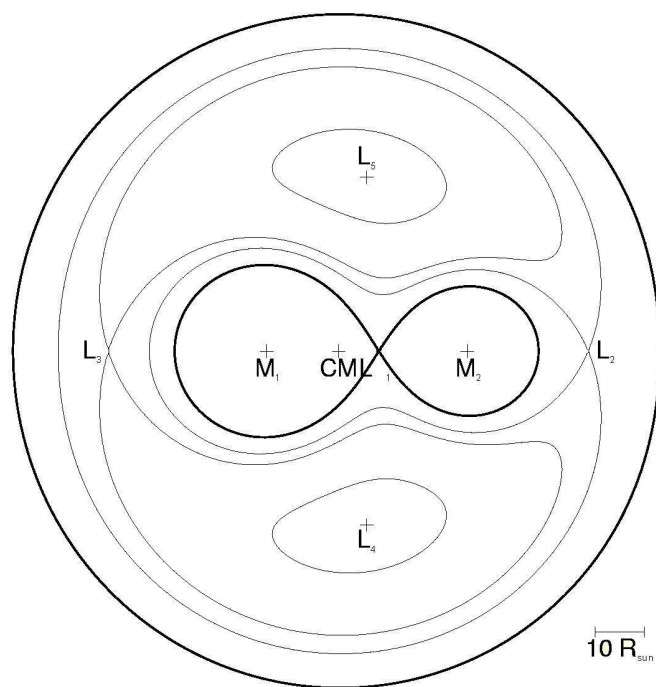


Figure 1.1: Roche lobe diagram

Table 1.1: Physical properties of CVs that are discussed in this work from Downes et. al. (2001)

Object	Type	Period (day)(s)	Luminosity ¹ (log ₁₀ ergs s ⁻¹)	Other Name
AM Her	polar	0.128927	31.77 ²	3A 1815+498
BL Hyi	polar	0.078915	32.11 ²	H 0139-68
V834 Cen	polar	0.070498	31.72 ²	1E 1405-451
VV Pup	polar	0.069747	30.05 ³	1E 0812-1854
AO Psc	ip	0.149626(805.20)	32.57 ²	H 2252-035
BG CMi	ip	0.134748(847.03)	32.65 ⁴	3A 0729+103
EX Hya	ip	0.068234(4021.62)	31.79 ²	1E 1249-2858
FO Aqr	ip	0.20206(1254.45)	32.85 ²	H 2215-086
GK Per	ip	1.9968(351.34)	33.04 ³	BD +43 740a
PQ Gem	ip	0.216359(833.40)	32.79 ²	RE 0751+14
TV Col	ip	0.228599(1911)	33.08 ²	2A 0526-328
TX Col	ip	0.2383(1911)	32.71 ²	H 0542-407
V1223 Sgr	ip	0.140244(746.)	33.73 ²	3A 1851-312
XY Ari	ip	0.252697(206.298)	33.77 ²	H 0253+193
YY Dra	ip	0.165374(529.31)	31.82 ³	DO Dra

Table 1.2: Physical properties of CVs cont'd from Table 1.1

Object	Type	Period (day)(s)	Luminosity (log ₁₀ ergs s ⁻¹)	Other Name
TW Pic	non-magnetic	0.2525 (7560) ¹¹	32.90 ⁵	H 0534-581
SS Cyg	non-magnetic	0.27513	32.08 ³	BD +42 4189a
TT Ari	non-magnetic	0.13755	31.40 ⁶	BD +14 341
U Gem	non-magnetic	0.176906	31.44 ³	BD +22 1807
V603 Aql	non-magnetic	0.1385	32.48 ³	HD 174107
WW Cet	non-magnetic	0.1758	32.04 ⁷	HV 8002/PHL 718
CP Tuc	polar	0.061832	27.70 ⁸	Tuc2, AX J2315-592
V1025 Cen	ip	0.05876(2146.53)	32.36 ²	RX 1238-38
V2400 Oph	ip	0.142(927.6)	34.44 ⁹	Oph3, RX J1712.6-2414
V1432 Aql	polar	0.140235	32.15 ¹⁰	Aql1, RX J1940-1025
V2301 Oph	polar	0.07845	31.90 ²	Oph1, 1H 1752+081
V1062 Tau	ip	0.41284(3726)	33.51 ²	Tau1, 1H 0459+246

¹ Luminosities are between 2-10 keV

¹¹ Periods are uncertain

REFERENCES - (2)Sazonov, S. et al. 2006; (3)Baskill, D. S. et al 2004; (4)Warner, B. 1995; (5)Patterson, J. 1994; (6)Greiner, J. 1998; (7)Pandel, D. 2005; (8)Ramsay, G. 2006; (9)de Martino, et al. 2004; (10)Rana, V. R., et al. 2005.

PQ Gem, V1025 Cen and V2400 Oph distances taken as 500 pc.

Table 1.3: Timing properties of AXPs and SGRs.

Object	Period	Period Derivative	Magnetic Field	Spin Down Age
	(s)	(10^{-11} s s $^{-1}$)	(10^{14} Gauss)	(10^3 years)
SGR 0526-66 ¹	8.0	6.6	7.4	1.9
SGR 1627-41 ²	6.4?	-	-	-
SGR 1806-20 ³	7.5	8.3-47	7.8	1.4
SGR 1900+14 ⁴	5.2	6.1-20	5.7	1.3
CXOU 010043.1-721134 ⁵	8.0	-	-	-
4U 0142+61 ⁶	8.7	0.20	1.3	70
1E 1048.1-5937 ⁷	6.4	1.3-10	3.9	4.3
1RXS J170849-400910 ⁸	11.0	1.9	4.7	9.0
XTE J1810-197 ⁹	5.5	1.5	2.9	5.7
1E 1841-045 ¹⁰	11.8	4.2	7.1	4.5
AX J1844-0258 ¹¹	7.0	-	-	-
1E 2259+586 ¹²	7.0	0.048	0.60	220

REFERENCES (1)Kulkarni et al. 2003; (2)Woods et al. 1999a; (3),(4)Woods et al. 2002; (5)Lamb et al. 2003; (6)Gavriil & Kaspi 2002; (7)Kaspi et al. 2001; Gavriil & Kaspi 2004; (8)Gavriil & Kaspi 2002; (9)Ibrahim et al. 2004; (10)Gotthelf et al. 2002; (11)Gotthelf & Vasisht 1998; (12)Gavriil & Kaspi 2002

Table 1.4: Spectral properties of AXPs and SGRs. Luminosities are 2-10 keV integrated.

Source	NH	Blackbody Temperature	Photon Index	Luminosity \log_{10} (ergs s ⁻¹)
	10 ²² (cm ⁻²)	(keV)		
SGR 0526-66	0.55	0.53	3.1	35.41
SGR 1627-41	9.0	-	2.9	33.61-35
SGR 1806-20	6.3	-	2.0	35.50-35.73
SGR 1900+14	2.6	0.43	1.0-2.5	35.3-35.54
CXOU 010043.1-721134	0.14	0.41	-	34.60
4U 0142+61	0.91	0.46	3.4	34.86
1E 1048.1-5937	1.0	0.63	2.9	33.63-34.40
1RXS J170849-400910	1.4	0.44	2.4	35.28
XTE J1810-197	1.1	0.67	3.7	35.27
1E 1841-045	2.5	0.44	2.0	35.04
AX J1845-0258	9	-	4.6	33.70-35.08
1E 2259+586	1.1	0.41	3.6-4.2	34.24-34.78

REFERENCES (1)Kulkarni et al. 2003; (2)Kouveliotou et al. 2003; (3)Mereghetti et al. 2000; (4)Woods et al. 2001; (5)Lamb et al. 2002; (6)Patel et al. 2003; (7) Mereghetti et al. 2004; (8)Rea et al. 2003; (9)Gotthelf et al. 2004; (10)Morii et al. 2003; (11)Gotthelf & Vasisht 1998; (12)Woods et al. 2004a.

CHAPTER 2

RXTE OBSERVATIONS AND DATA ANALYSIS

2.1 RXTE Observations

The purpose of this research is to discuss the variability properties of CVs and magnetars. To give a global account for the band limited noise and possible QPO properties of these objects we used 2 - 60 keV archived public data of Rossi X-Ray Timing Explorer RXTE (Brandt et al. 1993). This archive consists of public data of 55 CVs and 10 AXPs and SGRs. Taking into account the duration and count rates of the archival observations, we selected 27 CVs and 5 AXP or SGR sources. The data were obtained by the Proportional Counter Array (PCA; Jahoda et al. 1996) instrument onboard RXTE. PCA instrument consists of five Proportional Counter Units (PCUs) which operate in the 2-60 keV range with a collecting area of 6500 cm². This instrument has a 1 degree field of view. The major contribution in the thesis work is fitting of the power spectra of CVs with powerlaw+lorentzian models and calculation of the Q values together with preparation of averaged power spectra in time of AXPs and SGRs from selected data sets to detect broad-band noise. A preliminary analysis of CVs is published

in Balman, Kulebi and Beklen (2006) and the detailed work is in progress in Balman et al. (2006).

We have generally used archived background subtracted and merged light curves (or data) from the standard data products in the R-XTE archive. Light curves with 16 second bins have been assumed for the CV analysis and Light curves were created from a set of 125 ms resolution background subtracted data for AXPs and SGRs. Only when necessary, particularly in some high and low states of CVs or to check background effects non-background subtracted light curves were created from original data using SEEXTRCT v4.2. The manipulation of the data was made with the FTOOLS v5.21 software and these data are available at "ftp.legacy.gsfc.nasa.gov."

The power spectral analysis of the light curves with various timing resolutions explained as above were obtained through FFT, using XRONOS v5.21 software. We searched noise in the 0.1 Hz to 0.0001 Hz frequency range. For CVs 1-2 ks long 30-100 frames were been averaged over in the low frequencies ($LFN; \nu < 0.01 Hz$). In high frequencies ($HFN; 0.01 < \nu < 1Hz$) 100-200 s long frames were averaged over 100-500 spectra. In the same high frequency range 256 s long frames were averaged for magnetars over 60-600 windows.

The power densities were expressed in terms of the fractional rms amplitude squared, and the expected white noise levels were subtracted to obtain the rms fractional variability of the time series ($(rms^2 - mean)/Hz$).

The CV power spectra were fitted using power law models with exponential cutoffs wherever necessary. Lorentzians were also added to model the QPOs. Their values and the power law indices were listed in tables 3.1 and 3.2.

For the magnetar spectra we correlated data epochs with the published burst dates, and also looked for other objects in the FOV. We recovered 1 known SGR and 4 known AXPs with unpolluted FOVs. These data were merged according to their burst information that gave us the opportunity to account for high and low activity variability, if there were any.

We also divided merged lightcurves into three month intervals so that the statistical quality of the averaged power spectra is adequate to look for broadband noise.

All observations that are used in this work are shown in tables 2.1 and 2.2, and lightcurves representing the high and low states of CVs and AXPs appear between figures 2.1 through 2.4. These lightcurves were plotted using `lcurve` command of XRONOS 5.1 software.

2.2 Fourier Techniques in X-ray Timing

The basic premise of the Fourier transform is to decompose the signal into sine functions. For a time dependent function $x(t)$, an array of different cosine functions with specific frequencies ω_j can be added together with an amplitude a_j , and phase ϕ_j .

$$x(t) = \frac{1}{N} \sum_j a_j \cos(w_j t - \phi_j) = \frac{1}{N} \sum_j [A_j \cos w_j t + B_j \sin w_j t] \quad (2.1)$$

The amplitudes of further decomposed cosine function can be calculated as

$$A_j = \sum_{k=0}^{N-1} x_k \cos w_j t \quad (2.2)$$

$$B_j = \sum_{k=0}^{N-1} x_k \sin w_j t \quad (2.3)$$

here x_k is $x(t_k)$, in which x_k represents a signal with the frequency w_j and the amplitudes are called the correlation of the signal. This means if a frequency is strong in a signal corresponding Fourier amplitude should also be strong. Practically x_k stands for the number of photons in bin k .

Using more convenient terms, they can be written in terms of complex numbers.

$$a_j = \sum_k^{N-1} x_k e^{iw_j t k} \quad (2.4)$$

$$x_k = \frac{1}{N} \sum_k^{N-1} a_j e^{-iw_j t k} \quad (2.5)$$

where a_j are complex Fourier amplitudes and they are Fourier transforms of the signal x_k . This notation is especially useful for a discrete series of signals with N bins.

$$a_j = \sum_{k=0}^{N-1} x_k e^{2\pi i k / N} \quad j = -\frac{N}{2}, \dots, \frac{N}{2} - 1 \quad (2.6)$$

$$x_k = \frac{1}{N} \sum_{j=-N/2}^{N/2-1} a_j e^{-2\pi i k / N} \quad k = 0, \dots, N-1 \quad (2.7)$$

the Fourier amplitudes can be negative because of the complex structure. There are N of both x_k and a_j . If this time series has its discrete values in every T length of time then the differential time step is $\delta t = T/N$. This also means that the differential frequency step is $\delta \nu = 1/T$. From here the duration for each signal x_k is defined as $t_k = kT/N$, and the frequency counterpart is $w_j = 2\pi \nu_j = 2\pi_j/T$ for a frequency series description.

The highest frequency that can be attained by this description is the half of the sampling frequency δt , which is called the Nyquist frequency $\nu_{N/2} = \frac{1}{2T}$.

The zero frequency gives the total number of photons detected,

$$a_0 = \sum_k x_k \quad (2.8)$$

Parseval's theorem states that,

$$\sum_{k=0}^{N-1} |x_k|^2 = \frac{1}{N} \sum_{j=-N/2}^{N/2-1} |a_j|^2 \quad (2.9)$$

which means that the summed square modulus of the signal and the total variance is equal to each other. Using this power can be defined by using Leahy normalization (Leahy et al., 1983) where N_{ph} is the total number of photons, a_0 . This can basically be represented by;

$$\frac{\frac{1}{N} \sum |x_k|^2}{\frac{1}{N} \sum N_{ph}} = \frac{N |a_j|^2}{N N_{ph}} \quad (2.10)$$

and considering the degree of freedom of 2, we end up with Leahy power:

$$P_j = \frac{2}{N_{ph}} |a_j|^2 \quad (2.11)$$

In this form of normalization the mean power is equal to two. There is also another type of normalization, where power is defined as rms^2/Hz (Miyamoto, et al. 1991). It can be reached with minor alterations to the Leahy normalization.

$$\frac{\sum |x_k|^2}{\frac{N_{ph}}{T} N_{ph}} = \frac{2 |a_j|^2}{N_{ph} \frac{N_{ph}}{T}} \quad (2.12)$$

Here N_{ph}/T is equal to the mean count rate R

$$\frac{2 |a_j|^2}{R N_{ph}} \quad (2.13)$$

The dominant problem in Fourier analysis is the effect background timing noise on the on the original signal. The step taken in order to rectify this deficiency is to derive an expression for the probability distribution of the noise $P_{j,\text{noise}}$. Most common assumption is based on the situation where $a_j = a_{j,\text{signal}} + a_{j,\text{noise}}$ and the noise is random uncorrelated noise, that is:

$$P_j = P_{j,\text{signal}} + P_{j,\text{noise}} \quad (2.14)$$

The noise power includes $A_{j,\text{noise}}$ and $B_{j,\text{noise}}$ Fourier amplitudes and this means P_j commutes with χ^2 distribution with 2 degrees of freedom. If the signal x_k is pure photon counting noise, then the probability to surpass a certain threshold is given by;

$$\text{Prob}(P_{j,\text{noise}} > P_{\text{threshold}}) = Q(P_{\text{threshold}}|2) \quad (2.15)$$

and the integral probability of χ^2 being,

$$Q(\chi^2|\nu) = \left[2^{\nu/2}\Gamma\left(\frac{\nu}{2}\right)\right]^{-1} \int_{\chi^2}^{\infty} t^{\frac{\nu}{2}-1} e^{-\frac{t}{2}} dt. \quad (2.16)$$

Since neither using a larger time window T nor using smaller time steps δt is useful in above expression there are different methods for increasing the signal to noise ratio for periodicity.

The first one of the two methods used for decreasing the large variance of the noise is to rebin the spectrum in W frequency bins and the other one is to average the power spectrum of M divided segments of the total data. The normalizations are according to equation (2.4) and the N_{ph} is the number of photons for each window. One caveat for these methods is that it degrades the frequency resolution. On the other hand the advantages of this method are that it saves more time and the averaging of different windows brings about the possibility of selectivity in spectra according to variability.

This method's advantage comes from χ^2 distributions additive property and the degree of freedom becomes $2MW$ in this scheme. This results in less noise

and with the below probability to extend a certain threshold,

$$\text{Prob}(P_{j,\text{noise}} > P_{\text{threshold}}) = Q(\text{MWP}_{\text{threshold}}|2\text{MW}) \quad (2.17)$$

with the integral probability,

$$Q_{\text{Gauss}}(x) = \frac{1}{\sqrt{2\pi}} \int_x^{\infty} e^{-\frac{t}{2}} dt. \quad (2.18)$$

Hence averaging powers presents considerable advantage in detecting and resolving different spectral stochastic morphologies.

The most commonly recognized morphology is a resolved peak in the spectrum which can be defined as a *quasi-periodic oscillations* (QPOs). These fluctuations have certain frequencies that are their centroid frequency of their peak and their coherence time is scaled by the relative width of the peak that is FWHM/centroid frequency. For a morphology to be defined as a QPO, its relative width should be smaller than 0.5 (Lewin 1996). The reason for the loss of coherence after the designated time can be due to frequency shifts or phase jumps in a continuous signal or the limited lifetime of a signal.

The QPO is a stochastic phenomenon and cannot be physically modeled without any other evidence. The reasons for the QPO phenomenon were modeled successfully as shot noise. But qualitatively the same effect can occur from frequency modulation, and from an oscillation with limited lifetime.

The next type of morphology is the band limited power law noise that is commonly referred to as *red noise*. Power law noise is described as;

$$P(\nu) = \frac{C}{\int_{\nu_1}^{\nu_2} \nu^\alpha} \nu^{-\alpha} \quad (2.19)$$

α is the power law index and C is the integral of the power spectrum between ν_1 and ν_2 . Fourier techniques are applicable up until $\alpha = 2$, if the power law index gets steeper, this means the spectrum may be suffering from low frequency leakage (Deeter & Boynton 1982). This means the power at the lower frequencies seem to be higher than it should be and this is a consequence of a very slow variability, that surpasses the observation length.

The physics behind these stochastic phenomena are numerous and can not be generalized to one single effect. So to explain broad-band spectra a general phenomenological approach is adopted by van der Klis (1988) for NSs and black holes. In this approach, description of accreting sources relies on information from color to color diagrams and power spectral information. In these sources the red noise power law indexes and cutoff frequencies are related to their accretion rates, \dot{M} , and their QPO frequencies are expressed with blob model in this picture. The oscillations are labeled according to their coherences, frequencies and the spectral state of the sources in the X-rays, namely the location of the sources on the color-color diagram. These oscillations are generally grouped as; kHz double QPOs, Horizontal Branch Oscillations(HBOs) and Normal Branch Oscillations (NBOs)(van der Klis, 2000). Z sources which are luminous LMXRBs show all

four kinds; double kHz in 200-1200 Hz, HBOs in 15-60 Hz, NBOs in 5-20 Hz.

While atoll sources, that are less luminous NS LMXRBs show only; double QPOs in 500-1250 Hz and HBOs in 20-60 Hz.

Table 2.1: Log of CV observations in this paper.

Source	OBS-ID	Length (ksec)	Date yyyymmdd	Source	OBS-ID	Length (ksec)	Date yyyymmdd
AM Her	80005-01	65.0	20030711	TW Pic	40009-01	17.8	19990705
AM Her	30007-01	34.0	19980804	SS Cyg	20033-01	84.0	19970301
BL Hyi	20013-03	50.0	19970924	SS Cyg	50011-01	180.0	20000305
V834 Cen	10016-02	20.0	19960319	TT Ari	30022-01	40.0	19981218
VV Pup	40006-03	32.4	20011210	U Gem	80011-01	400.0	20040227
AO PSC	20021-01	54.0	19970906	U Gem	20035-01	200.0	19971107
BG CMi	10033-01	100.0	19960414	V603 Aql	60013-01	60.0	20010417
EX Hya	50408-01	15310.0	20000518	WW Cet	30026-01	23.6	19980126
EX Hya	30016-01	80.0	19980810	CP Tuc	20015-01	96.00	19970719
FO Aqr	20022-01	100.0	19970514	V2400 Oph	50007-01	300.0	20000724
GK Per	10023-01	75.0	19960227	V1432 Aql	10025-01	75.00	19960712
PQ Gem	20021-02	60.0	19970127	V2301 Oph	20013-04	50.00	19970926
TV Col	10034-01	88.0	19960809	V1062 Tau	30018-01	60.00	19980216
TX Col	20024-01	62.0	19970325	XY Ari	40008-01	80.0	19991029
V1223 Sgr	30019-01	80.0	19981130	YY Dra	10027-02	20.0	19960313
XY Ari	40008-01	80.0	19991029	YY Dra	40431-01	TOO	19990922

Table 2.2: AXPs and SGRs analyzed in this work.

Object	Observation	Count Rate	Maximum	Burst ¹
	Id		Count Rate	
1E 1048-5937	50082-04	3.771±10.07	54.01	no
1E 1048-5937	60069-03	3.302±10.41	126.7	yes
1E 1048-5937	70094-02	7.030±11.33	89.46	no
1E 1048-5937	80098-02	5.667±10.71	94.88	no
1E 2259+586	70094-01	2.695±13.17	1860.	yes
1E 2259+586	80098-01	1.765±11.34	92.31	no
1E 2259+586	90076-01	1.673±11.31	84.46	no
RXS J1708-40	90076-04	13.38±13.09	164.8	no
1E 1841-045	90076-03	9.013±15.25	114.9	no
1E 1841-045	91070-03	9.006±14.64	94.15	no
SGR 1806-20	50142-01	7.626±15.35	6569.	yes
SGR 1806-20	50142-03	7.607±11.62	247.0	yes
SGR 1806-20	60121-01	7.053±15.65	3342.	yes
SGR 1806-20	70136-02	10.69±31.82	14040	yes
SGR 1806-20	90073-02	10.93±62.17	27470	yes
SGR 1806-20	90074-02	12.70±98.64	26090	yes

¹ Observation dates have ben correlated with the The Gamma ray bursts

Coordinates Network (http://gcn.gsfc.nasa.gov/gcn3_archive.html) burst data.

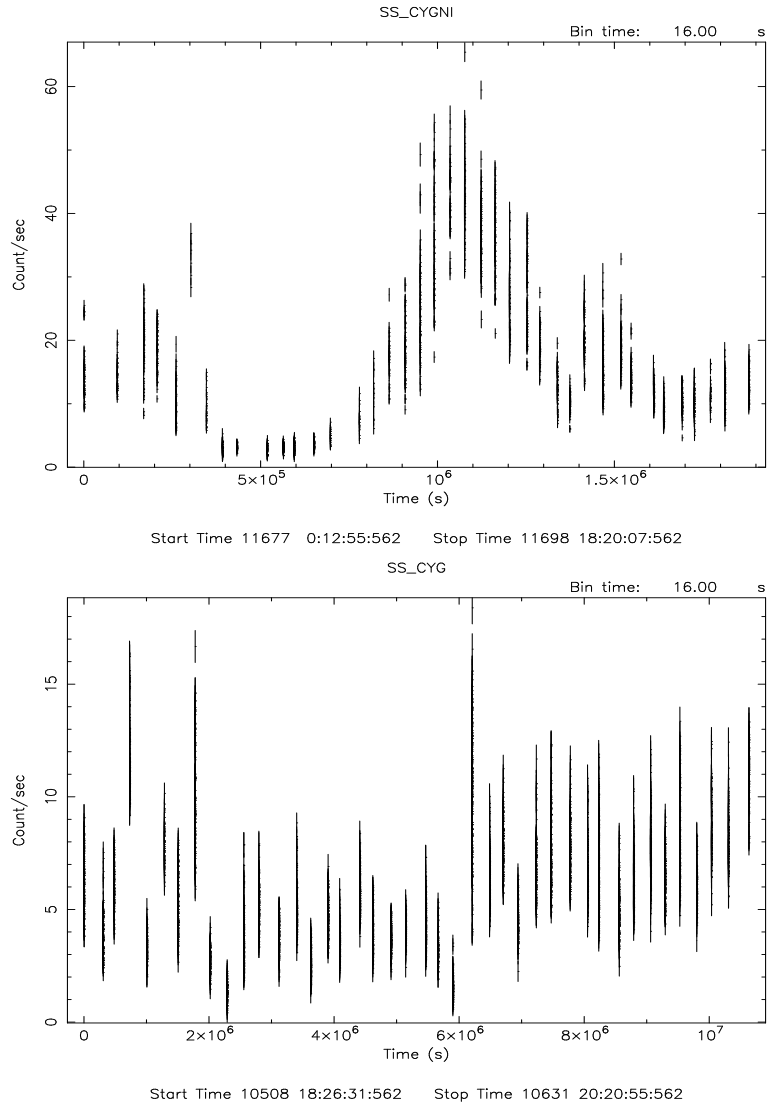


Figure 2.1: High versus low state lightcurve of SS Cyg
 50011-01(top) and 20033-01(bottom)lightcurves correspond to high and low states respectively.

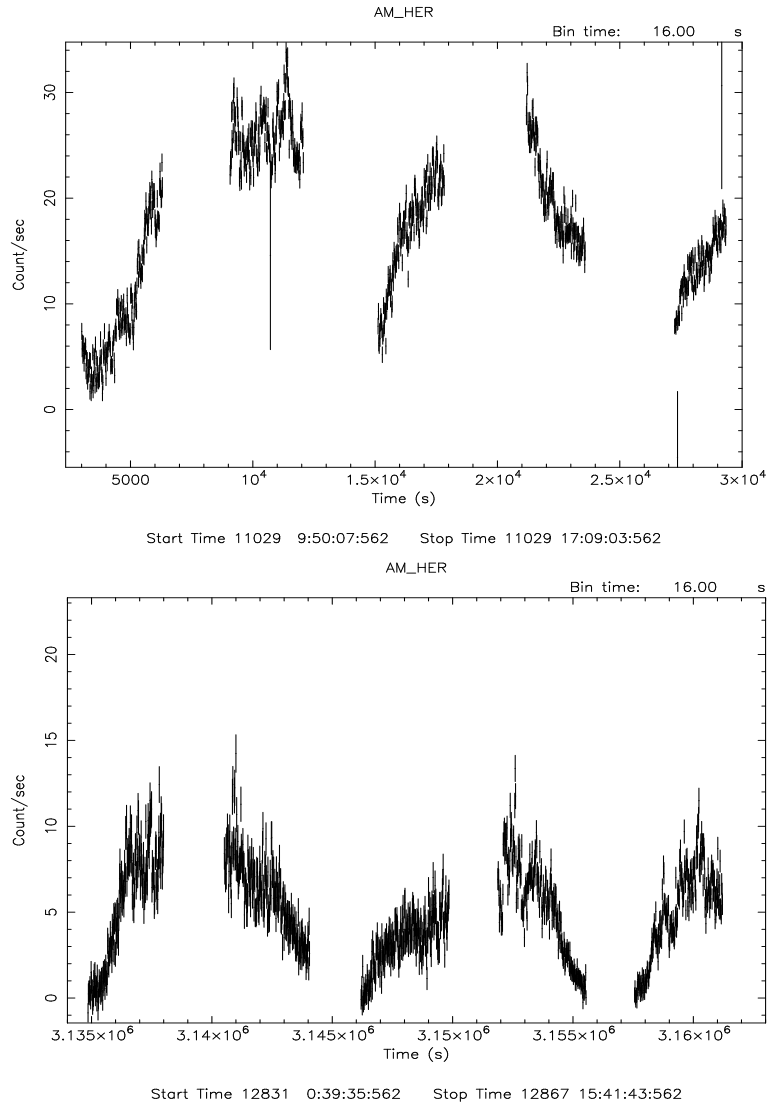


Figure 2.2: High versus low state lightcurve of AM Her
 30007-01(top) 80005-01(bottom) lightcurves correspond to high and low states respectively.

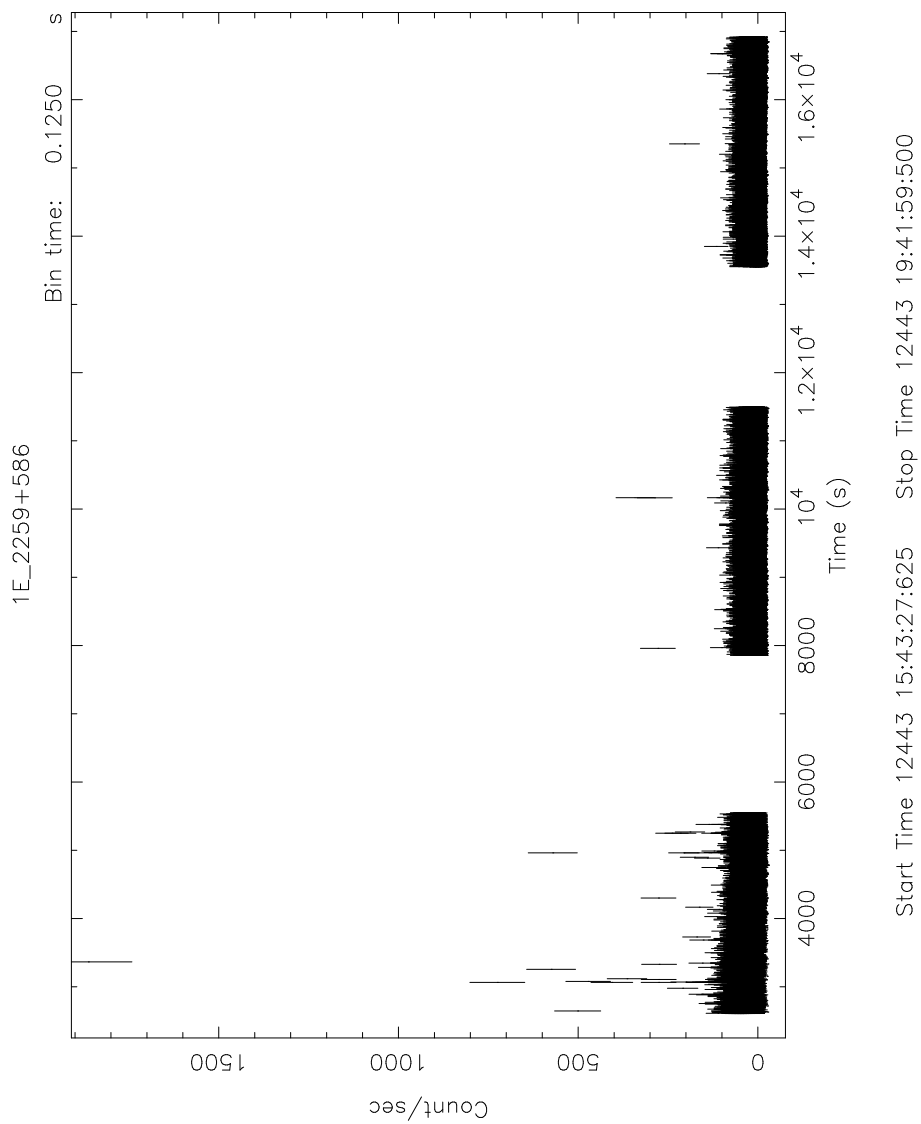


Figure 2.3: Burst epoch lightcurve of 1E 2259+586. Plot originally appeared in Kaspi & Gavriil, 2002.

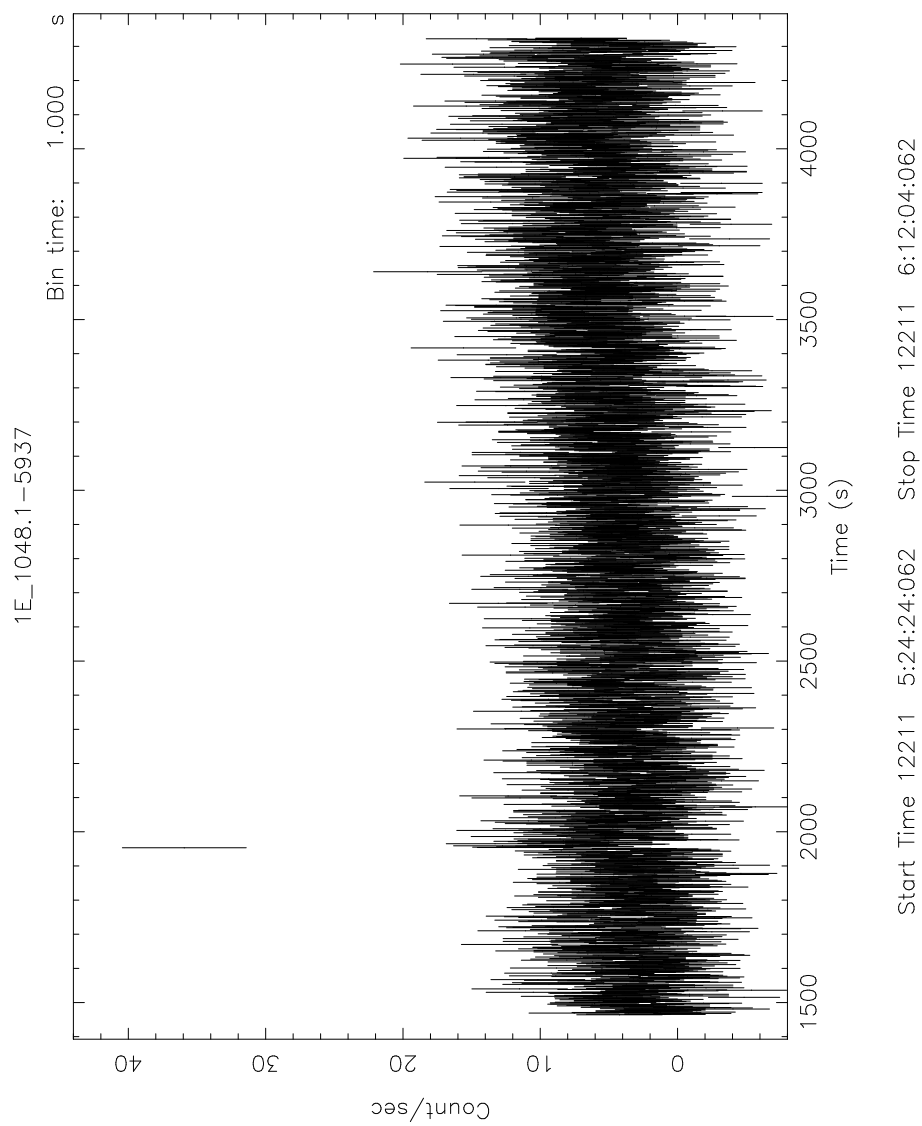


Figure 2.4: Burst epoch lightcurve of 1E 1048-5937

CHAPTER 3

RESULTS

3.1 Results for CVs

All CV spectra fitted with power law with exponential cutoffs or Lorentzians wherever necessary. Majority of these power law indices are between $-1.2 - -2.0$. Intermediate Polars have steep spectra with the exception of YY Dra. Some Polars and non-magnetic CVs have flattening in their spectra below 0.001 Hz.

3.1.1 Polars

In this work seven polars out of thirteen were investigated using the RXTE archive. Three objects; AM Her, V834 Cen, V1432 Aql showed QPOs.

Another important point is the change of the power law index because of the variation in the state of AM Her. This results from the fact that in the high state of AM Her the noise is concentrated in the high state, whereas in its quiescent state the red noise is in the lower frequencies.

3.1.2 Intermediate Polars

We analyzed the RXTE time series of 13 IPs. From these sources, EX Hya, PQ Gem, GK Per, V1025 Cen, V1062 Tau and YY Dra showed timing variability. YY Dra was especially hard to model since its high state was nearly flat and its quiescence state could only be modeled with three lorentzians.

3.1.3 Non-magnetic CVs

We were unable to model U Gem due to low statistics which is one of the more important non-magnetic sources. The most interesting result was the variable noise that has been observed in SS Cyg. The red noise shift in the frequency band from higher to lower frequencies as the state of the source changes is also observed for SS CYG. The high frequency red noise of high state, switches to low frequency red noise. This can also be identified with QPO exchange behavior. While quiescence state of SS Cyg has QPOs in its LF, in its high state QPOs are seen in HF.

3.2 Results for AXPs and SGRs

This type of objects exhibit flat noise with a break which may be considered as band limited noise. In this investigation we were able to identify this flat noise with a definite cutoff, which presented to have different values of rms^2/Hz noise

depending on the object and its burst phases.

We sampled the RXTE data for these objects in three month long segments which increased the statistical quality of the power spectra. The burst intervals were excluded from our data samples in order to avoid additional red noise because of the light curve variability during bursts.

In figures 3.5 through 3.12, three months long spectra are included in each panel. Each consecutive spectra are separated by 5 - 900 days which are also included in the figures.

We noted important activity epochs for each source. For 1E 1048-5937 and 1E 2259+586 this was their burst epochs, and their noise properties acts quite differently. While the steady $1 \text{ rms}^2/\text{Hz}$ noise of 1E 1048-5937 seems to drop by a factor of 10 right after the burst for three months then it recovers throughout the next three years until it reaches its former noise level. But 1E 2259+586 develops a noise in $10 \text{ rms}^2/\text{Hz}$ level right after its burst active state for nearly 2 years, until it recovers also back to its original low noise levels.

When we investigated the averaged power spectra of the two AXPs 1E 1841-04 and RXS J1708-40 we observed that they generally maintain a consistent higher noise level compared with the other two AXPs. The total time span of this excess broad-band noise is 1 year for RXS J1708-40, and 18 months for 1E 1841-04 in our investigation. 1E 1841-04 also stands out as the noisier of the two. This result

consistent with the increased white noise ¹ reported for this source by Gotthelf (2002).

¹ This applies for $f > 10^7$ Hz. (see Fig. 3.10) Gotthelf (2002) investigated the Lomb-Scargle periodogram (Press et al. 1992) power spectrum of a phase connected lightcurve of 1E 1841-04.

Table 3.1: Parameters and QPOs derived from the fits applied on the power spectra using Lorentzian and Power Law models

Source	OBS-ID	Rate (c/s)	Power Law Index ¹	QPO Centroid (Hz)	Q	State
AM Her	80005-01	5.21±3.59	-1.93 ^{+0.10} _{-0.20}	0.0074 ^{+0.0008} _{-0.0003}	184 ⁺¹³⁸ ₋₁₂₉	low
AM Her	30007-01	12.12±4.73	-1.78 ^{+0.10} _{-0.11}			
BL Hya	20013-03	1.60±0.94	-1.65 ^{+0.32} _{-0.16}			high state
V834 Cen	10016-02	1.68±0.31	-1.47 ^{+0.23} _{-0.36}	0.097 ^{+0.003} _{-0.004}	4.89 ^{+1.95} _{-1.28}	low
VV Pup	40006-03	0.23±0.44	-1.75 ^{+0.25} _{-0.75}			
AO PSC	20021-01	4.16±1.4	-0.86 ^{+0.18} _{-0.17}			
BG CMi	10033-01	2.91±1.51	-1.06 ^{+0.09} _{-0.11}			high state
EX Hya	50408-01	8.68±1.9	-1.34 ^{+0.02} _{-0.02}	0.0051 ^{+0.0002} _{-0.0001}	27.0 ^{+17.5} _{-7.0}	quiescence
				0.0089 ^{+0.0002} _{-0.0002}	10.0 ^{+6.40} _{-3.02}	
EX Hya	30016-01	16.55±9.04	-1.36 ^{+0.10} _{-0.10}			outburst
FO Aqr	20022-01	3.74±1.57	-1.37 ^{+0.05} _{-0.05}			
GK Per	10023-01	18.8±6.52	-1.44 ^{+0.06} _{-0.06}	0.089 ^{+0.003} _{-0.003}	8.59 ^{+4.91} _{-2.40}	outburst
				0.153 ^{+0.004} _{-0.003}	9.33 ^{+4.57} _{-2.45}	
PQ Gem	20021-02	2.25±0.45	-1.62 ^{+0.27} _{-0.40}	0.086 ^{+0.003} _{-0.004}	47.6 ^{+26.1} _{-11.6}	quiescence
TV Col	10034-01	4.99±1.03	-0.85 ^{+0.20} _{-0.20}			
TX Col	20024-01	1.73±0.53	-1.86 ^{+0.17} _{-0.16}			
V1223 Sgr	30019-01	9.35±1.86	-1.26 ^{+0.05} _{-0.05}			

¹ The parameters are derived using background subtracted and merged RXTE PCA light curve and the reduced χ^2 of the fits were between 0.78-1.9 with d.o.f. (32-64)

Table 3.2: Parameters and QPOs cont'd from Table 3.1

Source	OBS-ID	Rate (c/s)	Power Law Index ¹	QPO Centroid (Hz)	Q	State
XY Ari	40008-01	1.36±0.77	-2.07 ^{+0.22} _{-0.21}			
YY Dra	10027-02	2.19±0.45		0.0074 ^{+0.0008} _{-0.0003}	74.0 ^{+49.0} _{-19.8}	quiescence
YY Dra	40431-01	19.2±8.32	-1.47 ^{+0.13} _{-0.13}			outburst
TW Pic	40009-01	2.06±0.99	-1.47 ^{+0.14} _{-0.15}			
SS Cyg	20033-01	5.94±2.70	-1.88 ^{+0.36} _{-0.70}	0.0039 ^{+0.0030} _{-0.0014}	2.5 ^{+3.3} _{-1.27}	quiescence
				0.0067 ^{+0.0005} _{-0.0004}	8.03 ^{+4.47} _{-1.73}	quiescence
				0.0103 ^{+0.0001} _{-0.0001}	39.6 ^{+46.3} _{-13.3}	quiescence
SS Cyg	50011-01	16.5±11.4	-1.60 ^{+0.02} _{-0.02}	0.0087 ^{+0.0007} _{-0.0007}	9.63 ^{+19.2} _{-4.19}	outburst
TT Ari	30022-01	0.14±0.28	-0.21 ^{+0.16} _{-0.23}			
U Gem	80011-01	2.81±1.45				outburst
U Gem	20035-01	1.29±0.93				outburst
WW Cet	30026-01	1.24±0.52	-1.28 ^{+0.38} _{-0.25}			quiescence
V603 Aql	60013-01	2.98±0.89	-1.28 ^{+0.13} _{-0.13}			quiescence
CP Tuc	20015-01	1.939 ±0.838	-1.75 ^{+0.14} _{-0.24}			
V1025 Cen	20025-01	1.34 ±0.417	-2.41 ^{+0.04} _{-0.04}	0.0051 ^{+0.0001} _{-0.0001}	107 ^{+58.9} _{-21.9}	quiescence
V2400 Oph	50007-01	9.66 ±1.73	-1.32 ^{+0.02} _{-0.02}			
V1432 Aql	10025-01	1.08 ±0.982	-1.78 ^{+0.06} _{-0.16}	0.00399 ^{+0.0001} _{-0.0.0003}	97.3 ^{+57.1} _{-20.3}	quiescence
V1432 Aql	30009-05	3.41 ±2.17	-2.30 ^{+0.22} _{-0.11}			high state
V2301 Oph	20013-04	2.84 ±2.04	-1.70 ^{+0.02} _{-0.02}			
V1062 Tau	30018-01	2.65 ±1.01	-1.62 ^{+0.03} _{-0.02}	0.0096 ^{+0.0003} _{-0.0002}	16.1 ^{+18.9} _{-4.0}	quiescence

¹ The parameters are derived using background subtracted and merged RXTE PCA light curve and the reduced χ^2 of the fits were between 0.78-1.9 with d.o.f. (32-64)

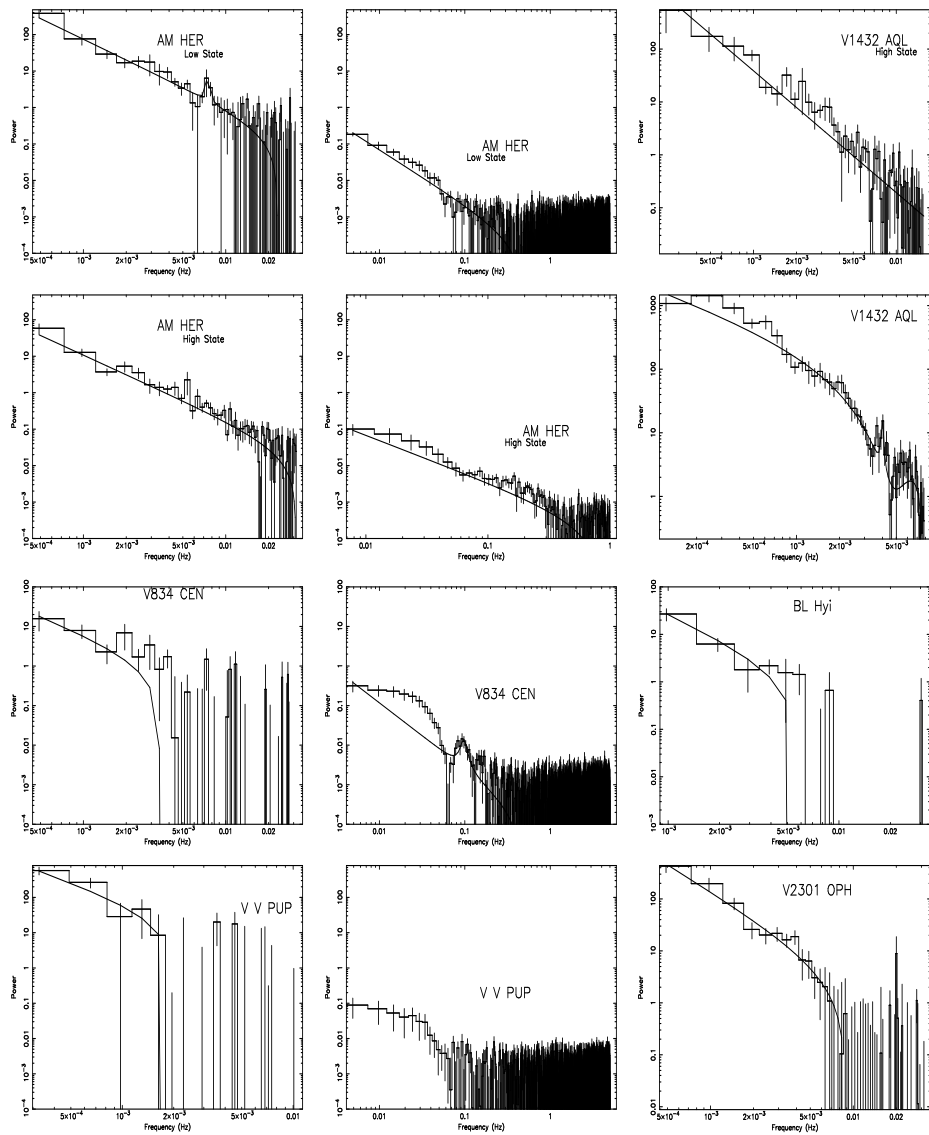


Figure 3.1: Broad-band noise of polars.

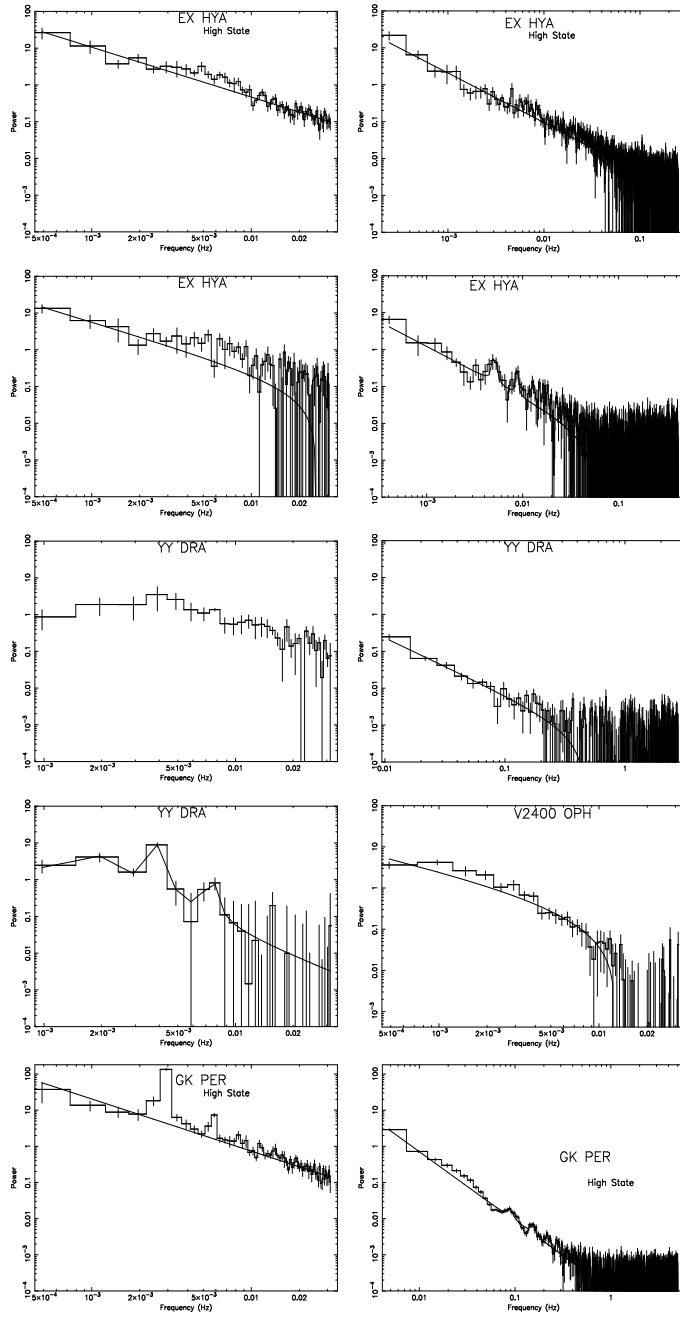


Figure 3.2: Broad-band noise of intermediate polars.

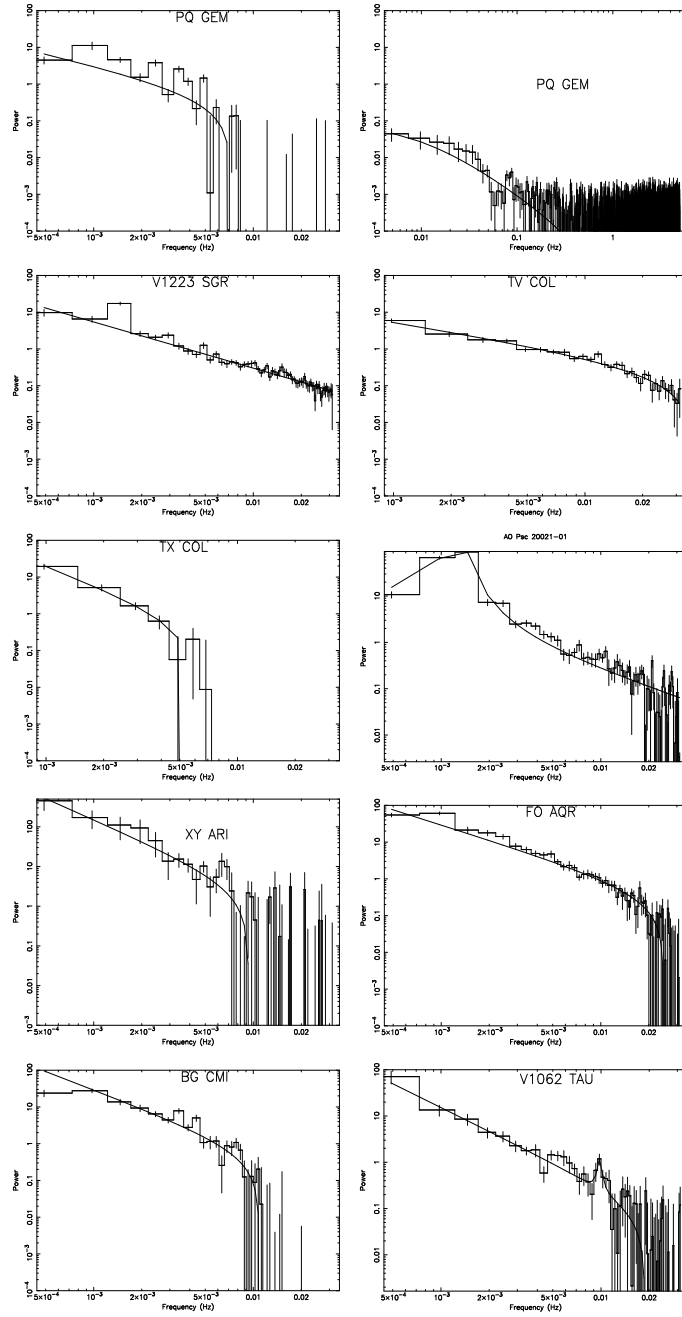


Figure 3.3: Broad-band noise of intermediate polars(cont'd).

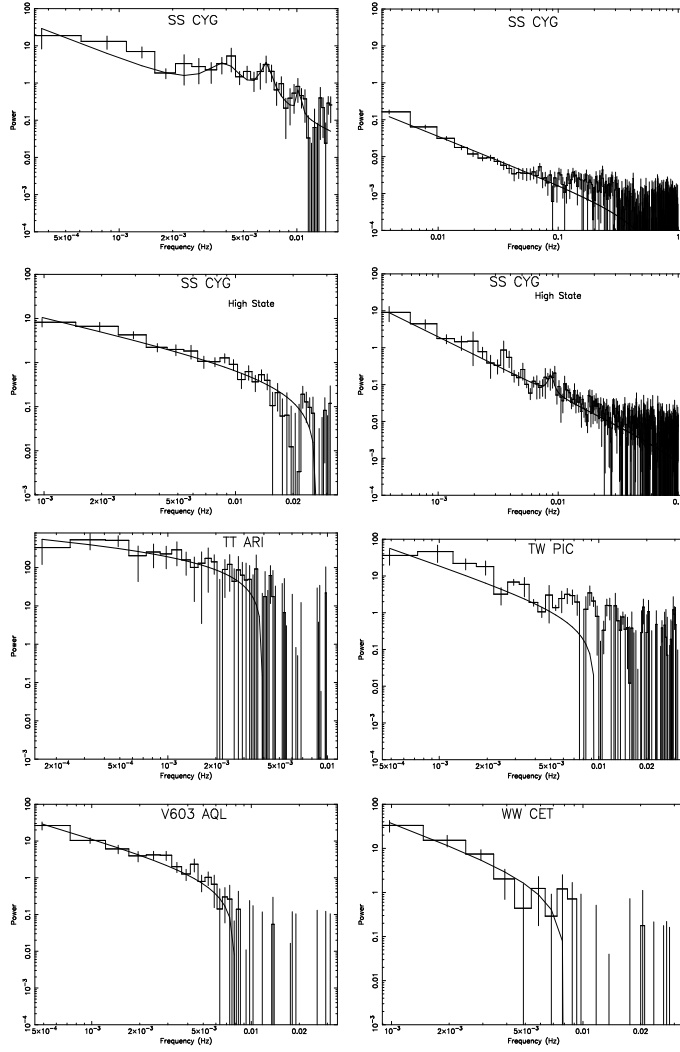


Figure 3.4: Broad-band noise of non-magnetic CVs.

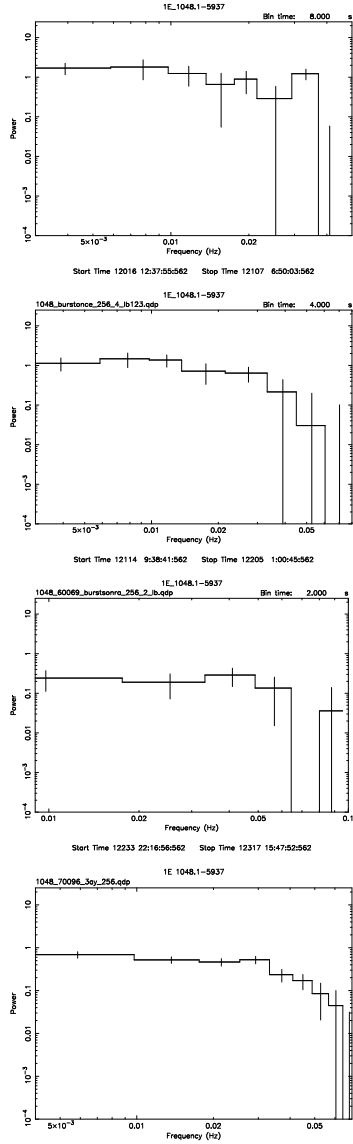


Figure 3.5: Broad-band noise of AXP 1E 1048-5937
 Start Times (MJD) - 52008, 52114, 52233, 52430
 Interval Separation (days)- 6, 3, 113, 58
 Burst Epochs (MJD) - 52211, 52227 (Kaspi & Gavriil 2003)

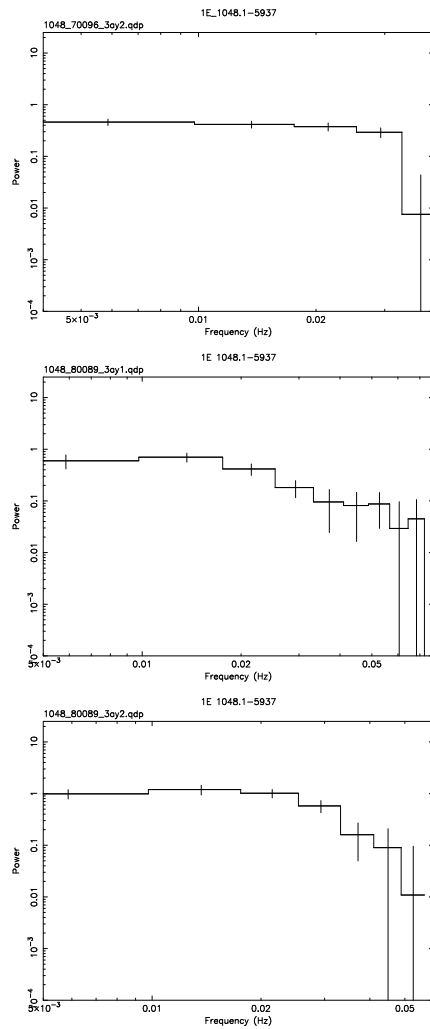


Figure 3.6: Broad-band noise of AXP 1E 1048-5937 (cont'd)
 Start Times (MJD) - 52584, 52734, 52962
 Interval Separation (days)- 63, 139

Figure 3.7: Broad-band noise of 1E 2259+586

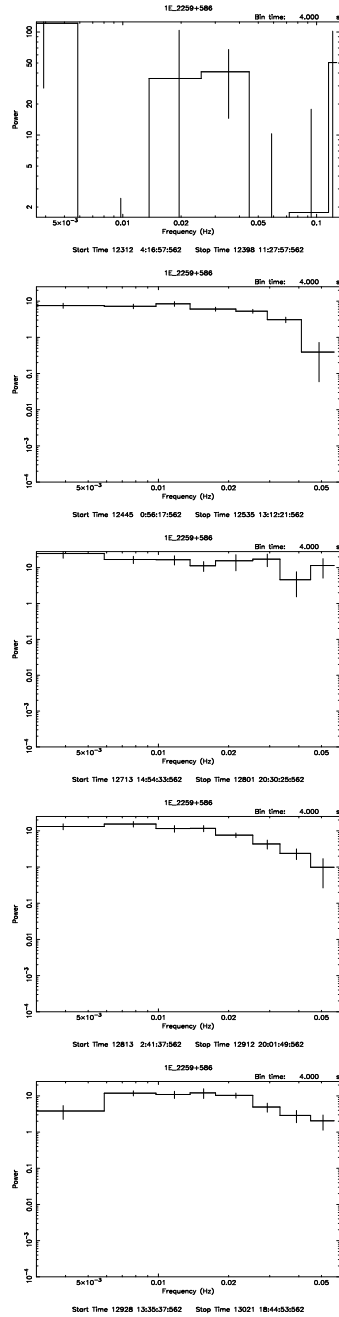


Figure 3.8: Broad-band noise of 1E 2259+586
 Start Times (MJD) - 52312, 52445, 52713, 52813, 52928
 Interval Separation (days)- 43, 13, 45, 12, 122
 Burst Epoch (MJD) - 52443 (Kaspi & Gavriil 2002)

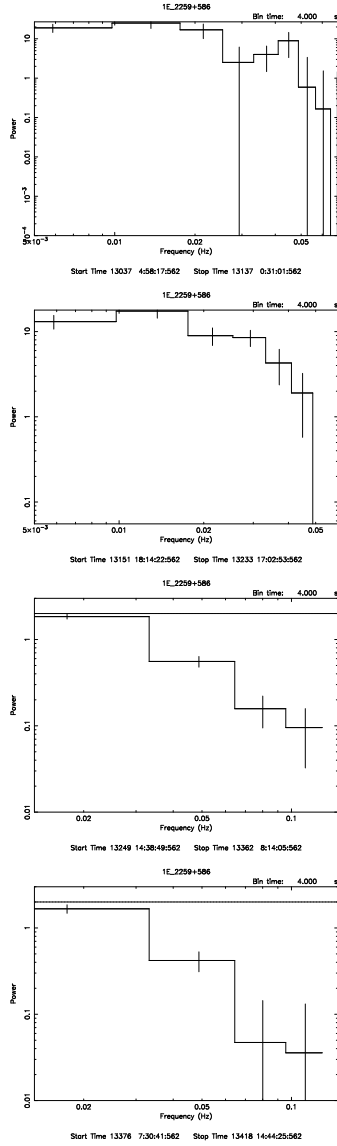


Figure 3.9: Broad-band noise of 1E 2259+586 (cont'd)
 Start Times (MJD)- 53037, 53151, 53362, 53418
 Interval Separation (days)- 15, 28, 14

The last two plots are Leahy normalized with the noise level at 2 to show that noise in this state is lower than mean.

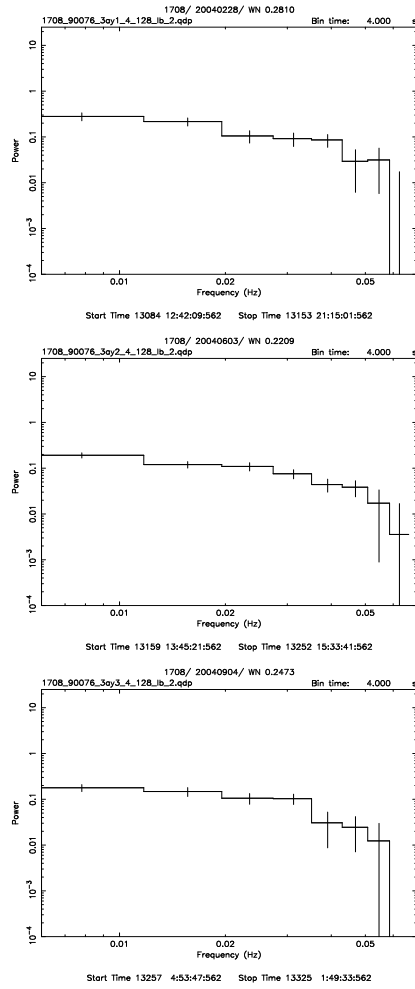


Figure 3.10: Broad-band noise of RXS J1708-40
 Start Times (MJD)- 53063, 53159, 53257
 Interval Separation (days)- 5, 5
 Glitcg Epochs (MJD) - 51444,601; 52014,177 (Kaspi & Gavriil 2003)

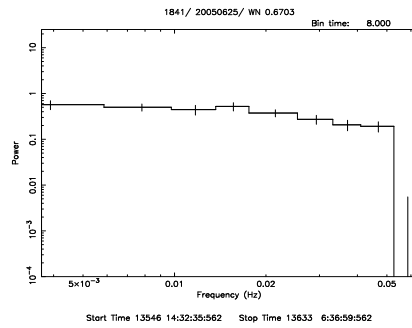
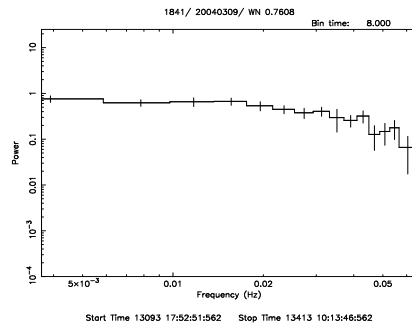
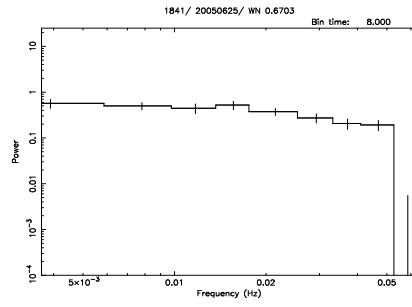


Figure 3.11: Broad-band noise of 1E 1841-045
 Start Times (MJD)- 53073, 53440, 53583
 Interval Separation (days)- 219, 15

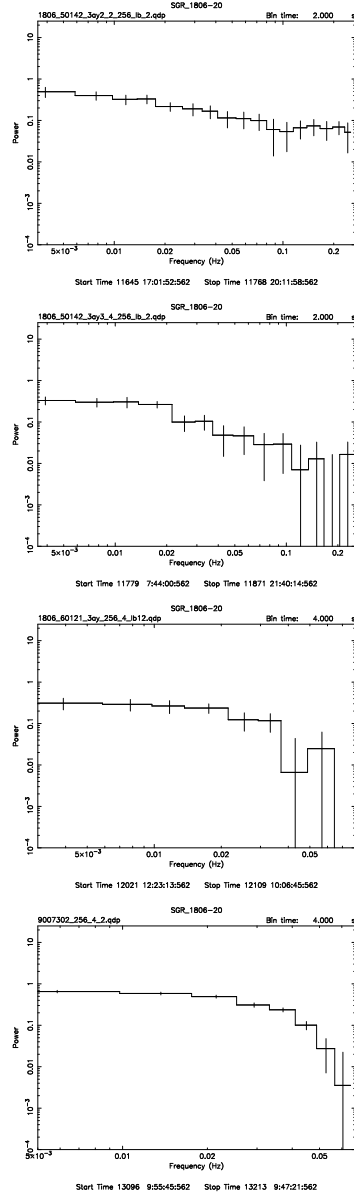


Figure 3.12: Broad-band noise of SGR 1806-20
 Start Times (MJD)- 51620, 51779, 51960, 53078
 Interval Separation (days)- 11, 87, 935

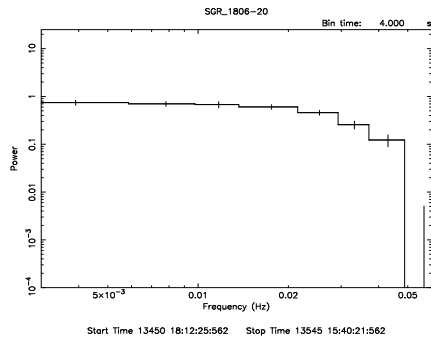
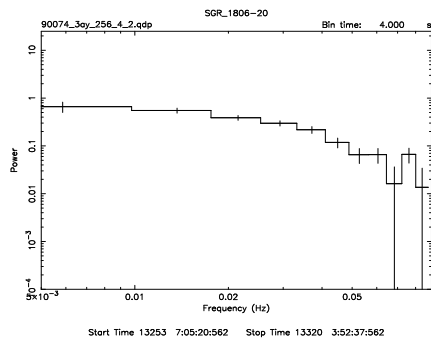
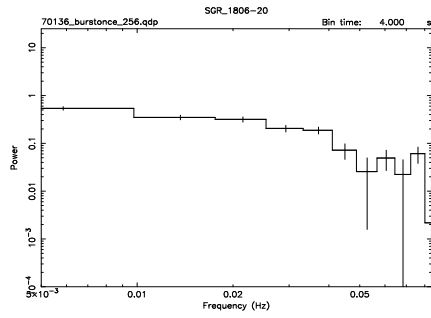


Figure 3.13: Broad-band noise of SGR 1806-20(cont'd)
 Start Times (MJD)- 53245, 53253, 53450
 Interval Separation (days)- 30, same interval with last one, 122 Giant Burst
 Epoch (MJD) - 53701

CHAPTER 4

CONCLUSION

4.1 CVs

The most important outcome of this investigation is the noise structure similarity between CVs and XRBs. The difference is that CV noise occur in much lower frequencies. Low frequency noise (LFN) of XRBs are high frequency noise (HFN) of CVs.

QPOs that are found during higher states were in the HFN range as detected in GK Per, V834 Cen and SS Cyg. From the data of EX Hya, SS Cyg, AM Her and YY Dra we can see that low/quiescent state QPOs are observed in LFN range. These LFN QPOs should be the equivalent of HBOs in LMXBs.

We do not recover most of SS Cyg QPOs particularly detected in the outburst stage. The QPOs we find are in the quiescent state. The main reason is that these QPOs found during the outburst are actually LFN QPOs and exists more coherently in the low/quiescent state. We averaged about 100 spectra to obtain our final results which would average out any QPO with low coherency.

In accordance with the fact above, the most important discovery was the

reallocation of noise in different states. During the high states of CVs HFN noise increases whereas in their low/quiescent states LFN dominates. This is very similar to the XRB behaviour, in which broad-band noise is controlled by the accretion rate. Hence it can be deduced that high and low states are due to changes in accretion rate.

The oscillation similarities between LMXRBs and CVs can be exemplified with the Dwarf Novae Oscillation(DNO) and double kHz QPO connection. From Warner & Woudt (2004) we know that CVs have highly coherent 8-40 s oscillations during their burst active phases. They also show slower oscillations at these states, which are approximately four times slower than DNOs and they are called longer period DNOs(lpDNOs). Phenomenologically these lpDNOs and DNOs connects with double kHz QPOs through their QPO or HBO frequencies respectively. The same relationship between ν_{HBO}/ν_{kHz} reported by Belloni, Psaltis, van der Klis (2002) have observed in ν_{QPO}/ν_{DNO} relation which is approximately 15 (Warner & Woudt 2004).

If we were to assume that LMXRB beat-frequency models(Alpar & Shaham 1985) also apply for CVs, we can say that DNOs occur in the innermost Keplerian frequency of the accretion disk. If we make a rough estimate from Keplerian frequency(Mauche 2002), $\nu_K = (1/2\pi)(GM/r^3)^{1/2}$

$$\frac{\nu_{WD}}{\nu_{NS}} = \left(\frac{M_{WD}}{M_{NS}}\right)^{1/2} \left(\frac{r_{NS}}{r_{WD}}\right)^{3/2} \quad (4.1)$$

and plug in parameters for both neutron stars and white dwarfs, as $M_{WD}/M_{NS} \approx$ and $r_{NS}/r_{WD} \approx 10\text{km}/5.5 \times 10^3\text{km}$ we end up with $\nu_{WD} \approx 10^{-4}\nu_{NS}$ for the inner region of the accreting source. This suggests the kHz QPOs and 0.1 Hz DNOs are analogous.

HBO frequencies are thought occur due to the beat-frequency between the spin and Keplerian frequency at a specific radius on the disk, e.g. the magnetospheric radius(Alpar & Shaham 1985). Although the physics taking place on the accretion disk of CVs differ with respect to the LMXRBs, this similarity points out to the structural similarity of these objects, namely the accretion disk.

4.2 AXPs and SGRs

The broad-band noise changes in 1E 1048-5937 and 1E 2259+586 could be understood if we compare our results with the other information on them. First on the basis of torque noise, we know that while 1E 2259+586 is very quiet, 1E 1048-5937 is very noisy such that it can not be phase connected for long time intervals. This torque noise have been measured and found to be consistent with accreting sources (Baykal et al. 2000). We also know that accreting sources present a rich phenomenology of broad-band noise; so eventhough torque noise and broad-band noise are different, the noisy spin down behaviour can contribute to broad-band noise.

The post-burst behaviour of 1E 2259+586 consists of rapid spin down over

60 days, after a glitch (Woods et al. 2003) and an excess in infrared radiation (Hulleman 2001). In this period 1E 2259+586 shows broad-band noise above white noise levels.

For 1E 1048-5937 pulsed flux increases, there are significant changes in spin down rate and large flux variations occur (Gavriil & Kaspi 2004). In our work we discovered that during this period, there is a sudden decrease in the broad-band noise structure. Coincidentally the torque (specifically $\dot{\nu}$) values of 1E 1048-5937 also decrease, but we were unable to search for a quantitative correlation.

All this evidence point out to the correlation of broad-noise to all of the other physical outcomes of the burst. But still we cannot discriminate between whether these changes are magnetospheric or accretion related. Change of broad-band noise can be interpreted as accretion like in CVs, since these changes correlate with the onset of bursting intervals. On the other hand it can be argued that, these power spectral characteristics are related to the possible changes in the crust tectonics, superfluid interior and thus the magnetosphere that affects the spin dynamics and X-Ray emission (Woods et al. 2003).

The broad-band noise analysis is significantly important for understanding accretion process and also variability in the light curves of CVs, AXPs and SGRs. In this work we conclude that CVs should be on the low frequency end of the XRB phenomenological spectrum. For AXP/SGR we discovered that, these sources

have significant rms^2 variability in their spectra and should further be investigated.

REFERENCES

- [1] Alpar, M.A., 2001, ApJ., 554, 1245
- [2] Alpar, M. A. & Shaham, J. 1985, Nature, 316, 239
- [3] Balman, Ş., Külebi, B., Beklen, E., 2006, Proceedings of the "The X-Ray Universe", Noordwijk, v. 1, 237
- [4] Baskill, Darren S., Wheatley, Peter J.; Osborne, Julian P., 2005, MNRAS, 357, 626
- [5] Baykal, A. , Strohmayer, T., Swank, J., Alpar, M.A., Stark, M.J., 2000, MNRAS, 319, 205
- [6] Belloni, T., Psaltis, D., van der Klis, M., 2002, ApJ, 572, 392
- [7] Chatterjee P., Hernquist, L., Narayan, R., 2000, ApJ., 541, 367
- [8] Colpi, M., Ulrich, G., Page, D., 2000, 529, L29
- [9] Deeter, J.E. & Boynton, P.E. 1982, ApJ., 261, 337.
- [10] Dib, R., Kaspi, V., Gavriil, F., Woods, P., 2006, ATel #845
- [11] Duncan, R.C., Thompson C., 1992, ApJ., 392, L9
- [12] Duncan, R.C., Thompson C., 1996, "High velocity Neutron Stars", AIP Conf. Proc., Vol. 366, 111
- [13] Ekşi, K.Y., Alpar, M.A., 2003, ApJ, 599, 450
- [14] Ertan, Ü., Alpar M. A., 2003, ApJ, 593, L93
- [15] Ertan, Ü., Göğüş, E. & Alpar, M. A., 2003, ApJ, 640, 435
- [16] Ertan, Ü., M. H. Erkut, K. Y. Eksi, Alpar, M. A., arXiv:/astro-ph/0606259 v1
- [17] Fahlman, G. C., Gregory, P.C., 1981, Nature, 293, 202
- [18] Faulkner, J. 1971, ApJ, 170, L99

- [19] Frank, J., King, A. & Raine, D. 1992, "Accretion Power in Astrophysics", Cambridge Univ. Press, Cambridge
- [20] Gaensler, B., et al., 2001, ApJ, 559, 963
- [21] Gavriil, F.P., Kaspi, V.M., Woods, P.M., 2002, Nature, 419
- [22] Gavriil, F. & Kaspi, V.M. 2004, ApJ, 607, 959
- [23] Goldreich, P., Reisenegger, A., 1992, ApJ, 395, 250
- [24] Gotthelf, E.V. & Vasisht, G. 1998, New Astr., 3, 293
- [25] Gotthelf, E.V., et al., 2002, ApJ, 564, L31
- [26] Gotthelf, E.V., Halpern, J.P., Buxton, M, & Bailyn, C. 2004, ApJ, 605, 368
- [27] Gregory, P.C., Fahlman, G. C., 1980, Nature, 287, 805
- [28] Greiner, J., 1998, A & A, 336, 626
- [29] Howell, S. B., Nelson, L. A. & Rappaport, S. 2001, ApJ, 550, 897
- [30] Hulleman, F., et al. 2001, ApJ, 563, L49
- [31] Ibrahim, A.I., et al. 2004, ApJ, 609, L21
- [32] Illarionov, A.F., & Syunyaev, R.A., 1975, Pis'ma Astron. Zh., 4, 11
- [33] Israel, G.L., Covino, S., Perna, R., Mignani, R., Stella, L., Campana, S., Marconi, G., Bono, G., Mereghetti, S., Motch, C., Negueruela, I., Oosterbroek, T., Angelini, L., 2003, ApJ 589, L93
- [34] Israel, G.L., Belloni, T., Stella, L., Rephaeli, Y., Gruber, D. E., Casella, P., Dall'Osso, S., Rea, N., Persic, M., Rothschild, R. E., 2005, ApJ 628, L53
- [35] Jackson, J.D., 1998, "Classical Electrodynamics", Wiley, New York
- [36] Kaspi, V.M., Gavriil, F.P., 2002, IAU Circ. No. 7924
- [37] Kaspi, V. M., Gavriil, F. P., 2003, 596, L71
- [38] Kaspi, V. M., et al., 2003, 588, L93
- [39] Kopal, Z., 1959, "Close Binary Systems", Chapman Hall, London
- [40] Kouveliotou, C., et al. 2003, ApJ, 596, L79

- [41] Kulkarni, S.R. et al. 2003, ApJ, 585, 948
- [42] Lamb, R.C., Fox, D.W., Macomb, D.J., & Prince, T.A. 2002, ApJ, 574, L29
- [43] Lamb, D., Prince, T.A., Macomb, D.J., & Majid, W.A. 2003b, IAU Circ. 8220
- [44] Leahy, D.A., Darbro, W., Elsner, R. F., Weisskopf, M. C., Kahn, S., Sutherland, P. G., & Grindlay, J. E. 1983, ApJ, 266, 160
- [45] Lewin, H.G.W., van Paradijs, J., van den Heuvel, E., 1995, "X-Ray Binaries", Cambridge University Press, Cambridge
- [46] Lipunov, V.M. 1992, "Astrophysics of Neutron Stars", Springer-Verlag, Berlin Heidelberg
- [47] Mauche, C. W., 2002, ApJ, 580, 423
- [48] de Martino, D.; Matt, G.; Belloni, T.; Haberl, F.; Mukai, K., 2005, A&A, 415, 1009
- [49] Mereghetti, S., Cremonesi, D., Feroci, M., & Tavani, M. 2000, A&A, 361, 240
- [50] Mereghetti, S., et al. 2004, ApJ, 612, 408
- [51] Miyamoto S., Kimura K., Kitamoto S., Dotani T., Ebisawa K., 1991, ApJ 383, 784
- [52] Norton, A.J., Wynn, G. A., Somerscales, R. V., 2004, ApJ, 614, 349
- [53] Pandel, D., Córdova, F. A., Mason, K. O., Priedhorsky, W. C., 2005, A&A, 626, 396
- [54] Patel, S.K., et al. 2003, ApJ, 587, 367
- [55] Patterson, J., Raymond, J. C., 1985, ApJ, 292, 535
- [56] Patterson, J., 1994, PASP, 106, 209
- [57] Press, W. H., Teukolsky, S. A., Vetterling, W. T., & Flannery, B. P. 1992, "Numerical Recipes: The Art of Scientific Computing", Cambridge Univ. Press, Cambridge.
- [58] Ramaty, R., Bonazzola, S., Cline, T. L., Kazanas, D., Meszaros, P., Lingenfelter, R. E. 1980, Nature, 287, 122

- [59] Ramsay, G., Napiwotzki, R., Hakala, P., Lehto, H., 2006, arXiv:astro-ph/0606628 v1
- [60] Rana, V. R., Singh, K. P., Barrett, P. E., Buckley, D. A. H., 2005, A&A, 625, 351
- [61] Rea, N., et al. 2003, ApJ, 586, L65
- [62] Sazonov, S., Revnivtsev M., Gilfanov, M., Churazov, E., and Sunyaev, R., 2006, A&A, 117
- [63] Shakura, N. I., & Sunyaev, R. A. 1973, A&A, 24, 337
- [64] Strohmayer, T. E., Watts, A. L., 2005 ApJ, 632, L111
- [65] Thompson C., Duncan, R.C., 1995, MNRAS., 275, 225
- [66] Thompson C.,Blaes O., 1998, Phys. Rev. D 57, 3219
- [67] Van der Klis, M., 1988, Timing Neutron Stars ASI
- [68] Van der Klis, M., 1994, ApJ Supp., 92, no. 2 , 511-519
- [69] Van Paradijs, J., Taam, R.E., van der Heuvel, E.P.J., 1995, A&A., 299, L41
- [70] Verbunt, F., & Zwaan, C., 1981, A&A, 100, L7
- [71] Verbunt, F. 1982, Space Science Reviews, 32, 379
- [72] Wang, Z., & Chakrabarty, D., 2002, ApJ, 579, L33
- [73] Wang, Z., Chakrabarty, D. & Kaplan, D., 2006, Nature, 440, 772
- [74] Warner, B., 1995,"Cataclysmic variable stars", Cambridge Univ. Press, Cambridge
- [75] Warner, B. & Woudt, P.A., 2004, ASP Conf. Ser., San Francisco, Vol. 315, 85
- [76] Warner, B. & Woudt, P. A. 2002, ASP Conf. Ser., San Francisco, Vol. 261, 406
- [77] Woods, P.M., et al. 1999, ApJ, 519, L139
- [78] Woods, P.M., et al. 2001, ApJ, 552, 748
- [79] Woods, P.M., et al. 2004a, ApJ, 605, 378
- [80] Woods, P.M., Thompson, C., 2004b, arXiv:astro-ph/0406133 v1